



HAL
open science

Evolution of pH-sensitive transcription termination in *Escherichia coli* during adaptation to repeated long-term starvation

Sarah Worthan, Robert Mccarthy, Mildred Delaleau, Ryan Stikeleather,
Benjamin Bratton, Marc Boudvillain, Megan Behringer

► To cite this version:

Sarah Worthan, Robert Mccarthy, Mildred Delaleau, Ryan Stikeleather, Benjamin Bratton, et al.. Evolution of pH-sensitive transcription termination in *Escherichia coli* during adaptation to repeated long-term starvation. *Proceedings of the National Academy of Sciences of the United States of America*, 2024, 121 (39), 10.1073/pnas.2405546121 . hal-04765566

HAL Id: hal-04765566

<https://hal.science/hal-04765566v1>

Submitted on 4 Nov 2024

HAL is a multi-disciplinary open access archive for the deposit and dissemination of scientific research documents, whether they are published or not. The documents may come from teaching and research institutions in France or abroad, or from public or private research centers.





L'archive ouverte pluridisciplinaire **HAL**, est destinée au dépôt et à la diffusion de documents scientifiques de niveau recherche, publiés ou non, émanant des établissements d'enseignement et de recherche français ou étrangers, des laboratoires publics ou privés.



Distributed under a Creative Commons Attribution - NonCommercial - NoDerivatives 4.0
International License



Evolution of pH-sensitive transcription termination in *Escherichia coli* during adaptation to repeated long-term starvation

Sarah B. Worthan^{a,b,c}, Robert D. P. McCarthy^a, Mildred Delaleau^d , Ryan Stikeleather^e , Benjamin P. Bratton^{b,c,f,g} , Marc Boudvillain^d , and Megan G. Behringer^{a,b,c,f,1} 

Affiliations are included on p. 11.

Edited by Richard Lenski, Michigan State University, East Lansing, MI; received March 17, 2024; accepted August 19, 2024

Fluctuating environments that consist of regular cycles of co-occurring stress are a common challenge faced by cellular populations. For a population to thrive in constantly changing conditions, an ability to coordinate a rapid cellular response is essential. Here, we identify a mutation conferring an arginine-to-histidine (Arg to His) substitution in the transcription terminator Rho. The *rho* R109H mutation frequently arose in *Escherichia coli* populations experimentally evolved under repeated long-term starvation conditions, during which the accumulation of metabolic waste followed by transfer into fresh media results in drastic environmental pH fluctuations associated with feast and famine. Metagenomic sequencing revealed that populations containing the *rho* mutation also possess putative loss-of-function mutations in *ycdI*, which encodes a recently characterized transcription factor associated with pH homeostasis. Genetic reconstructions of these mutations show that the *rho* allele confers plasticity via an alkaline-induced reduction of Rho function that, when found in tandem with a $\Delta ycdI$ allele, leads to intracellular alkalization and genetic assimilation of Rho mutant function. We further identify Arg to His substitutions at analogous sites in *rho* alleles from species that regularly experience neutral to alkaline pH fluctuations in their environments. Our results suggest that Arg to His substitutions in Rho may serve to rapidly coordinate complex physiological responses through pH sensing and shed light on how cellular populations use environmental cues to coordinate rapid responses to complex, fluctuating environments.

phenotypic plasticity | experimental evolution | alkaline stress | permissive mutation | transcription termination

Cellular populations regularly encounter fluctuating environmental stressors in their natural contexts, such as changes in resource availability, temperature, pH, and oxidative stress (1–3). This holds particularly true for microorganisms, which have evolved to thrive in some of Earth's most extreme and fluctuation-prone environments. Even in the most forgiving of habitats, microbial growth is primarily limited due, in part, to the scarcity of carbon and nitrogen sources and competition between microbes (4–6). Given that resource availability fluctuates temporally and spatially in natural environments (3), microbial growth in nature occurs in bursts as resources become accessible, resulting in long, stagnant periods of starvation punctuated by transient periods of growth, commonly referred to as feast/famine cycles (4, 7). Previous work has revealed several common microbial responses to persistent famine conditions, particularly those experienced by batch cultures during long-term stationary phase. These responses include an increase in genetic diversity, elevated mutation rates, morphological changes, and the emergence of the growth advantage in stationary phase (GASP) phenotype which confers an increased ability to catabolize alternative energy sources, such as amino acids, present in necromass as well as modulation of the stress response (8–14). Building upon this, recent work suggests that bacteria exhibit distinct responses depending on the frequency and magnitude of nutrient resource fluctuations, indicating that these fluctuations are an important determinant of bacterial behavior (3, 15–17). Notably, microbial populations subjected to cycles of prolonged starvation followed by a rapid influx of resources (i.e., 100-d feast/famine cycles) still exhibit GASP-like behavior but evolve mutations that are distinct from the mutations traditionally associated with the GASP phenotype (18). Thus, further investigation of how bacteria adapt to repeated nutrient resource fluctuations is critical to contextualizing microbial behavior in the wild.

Significance

We identified a pH-sensitive amino acid substitution that repeatedly arose in bacterial populations experimentally evolved under extreme cycles of starvation. This substitution affects the RNA binding of a transcription termination factor and bypasses traditional cell signaling to facilitate a rapid transcriptional response during alkaline/neutral pH shifts. As fluctuating conditions represent a universal challenge faced by macro- and microorganisms, pH-sensing mutations within RNA- or DNA-binding domains of global regulators represent an adaptation that can coordinate immediate cellular responses based on seasonal and recurring environmental cues.

Author contributions: S.B.W., B.P.B., M.B., and M.G.B. designed research; S.B.W., R.D.P.M., M.D., R.S., B.P.B., M.B., and M.G.B. performed research; R.S. contributed new reagents/analytic tools; S.B.W., R.D.P.M., M.D., B.P.B., M.B., and M.G.B. analyzed data; and S.B.W., R.D.P.M., B.P.B., M.B., and M.G.B. wrote the paper.

The authors declare no competing interest.

This article is a PNAS Direct Submission.

Copyright © 2024 the Author(s). Published by PNAS. This open access article is distributed under [Creative Commons Attribution-NonCommercial-NoDerivatives License 4.0 \(CC BY-NC-ND\)](https://creativecommons.org/licenses/by-nc-nd/4.0/).

¹To whom correspondence may be addressed. Email: megan.g.behringer@vanderbilt.edu

This article contains supporting information online at <https://www.pnas.org/lookup/suppl/doi:10.1073/pnas.2405546121/-/DCSupplemental>.

Published September 19, 2024.

Among the complications that microbes face in the wild, the reintroduction of nutrient resources into environments presents an inherent complex stress. Here, microbes must contend with additional stressors that coincide with nutrient resource replenishment, such as shifts in pH. Microbes are further challenged as they metabolize the newly introduced resources since excreted metabolic by-products can result in further environmental changes. These ecological feedbacks are also common in laboratory environments, particularly the significant pH fluctuations that can accompany growth (19). For example, when *Escherichia coli* populations are cultivated in the amino acid-based LB broth, their metabolic activities induce remarkable shifts in pH (20, 21). As these bacteria metabolize the amino acids for carbon, they release ammonia, causing the medium pH to undergo a dramatic transformation, shifting from a neutral pH of 7.0 to an alkaline pH of 9.0 in approximately 24 h (22, 23).

Consequently, many bacterial species have evolved mechanisms to sense and rapidly respond to changes in proton concentrations (24). For pathogens and marine bacteria which are frequently exposed to drastic shifts in external pH, the ability to sense these changes and respond through phenotypically plastic traits is critical to their survival (25–28). As such, microbes encode a number of systems dedicated to pH homeostasis, including amino acid-dependent acid resistance systems such as the GAD regulon in *E. coli* (29), two-component regulatory systems such as the MtrAB system in *Actinobacteria* (30) or the BatRS system in *Bartonella*, and one-component systems such as CadC in *E. coli* (31). Additionally, more global systems like the RpoS regulon control the expression of many components involved in the pH response (32). Experimental evolution under high-pH conditions has recapitulated the role of RpoS in the pH response through mutations, as well as revealed unexpected targets such as the two-component response regulator PhoB (33). Yet, another more universal plastic mechanism for pH sensing is the modulation of protein function via the protonation state of histidine residues, which is present across the Tree of Life. Histidine residues are often situated within functionally important sites of proteins, where their protonation status dictates the protein's functionality (34–36). The protonation state of histidine residues also regulates the activity of particular cell-surface receptors and transporters, such as G-coupled receptors (37) and ion transporters (38, 39). Moreover, tumorigenic arginine to histidine mutations are reported to contribute to cancers where they often confer pH sensing abilities (40, 41). Thus, histidine residues, acting as pH sensors, can serve as a plastic mechanism to enable rapid responses to changing environments.

One powerful approach for investigating how organisms navigate complex stresses and identifying the resulting mutations contributing to adaptation is experimental evolution (42, 43). Phenotypically plastic traits can evolve rapidly in evolution experiments and through these investigations, it has become evident that genes encoding global regulators of gene expression are frequent targets of selection when adapting to diverse environments, primarily due to their widespread impacts on various biological processes (44, 45). One such essential global regulator is Rho, which terminates transcription at hundreds of sites throughout the *E. coli* genome (46–49). Rho-dependent termination plays critical cellular roles, including the delineation of transcription unit boundaries and surveillance of the gene expression machinery (50), as well as involvement in many conditional gene regulatory mechanisms (51, 52). Additionally, Rho prevents unwanted transcription from loci antisense to genes or horizontally acquired genes, such as toxic prophage genes (46, 47). Functioning as a ring-shaped homohexamer, Rho utilizes its crown-like primary binding site to bind nascent transcripts at poorly conserved C-rich regions called *rut* (Rho

utilization) sites. Once bound to a *rut* site, the Rho hexamer guides the transcript into its central ring channel, where its secondary binding site mediates ATP-dependent [5' to 3'] movement along the RNA chain until Rho catches up with and dissociates RNA polymerase, effectively terminating transcription (53, 54).

Given the widespread prevalence of Rho-dependent termination in *E. coli*, any alteration in Rho function has the propensity to trigger extensive physiological changes. As such, numerous previous studies employing adaptive laboratory evolution under various conditions have reported nonsynonymous mutations in the *rho* gene. These conditions range from adaptation to heat stress (55–58) and exposure to copper (59) and ethanol (60, 61) to the utilization of various carbon sources (62, 63). Notably, previously reported adaptive mutations in *rho* exhibit variability, affecting residues distributed throughout the gene, particularly in regions associated with its core functions, including the primary and secondary binding site domains. Hence, the pleiotropic nature of Rho positions it as a frequently positively selected genetic target in *E. coli* when confronted with novel and intricate environmental challenges.

Here, we investigate a mutation in *rho* that results in an R109H substitution that fixed in 5 out of 16 *E. coli* populations during experimental evolution in repeated long-term starvation (RLTS) conditions consisting of 100 d between transfers into fresh LB-Miller broth (64). Each of these populations also contained putative loss of function mutations in an additional gene, *ydcl*, which encodes a poorly characterized transcriptional regulator related to pH homeostasis (65). Since arginine-to-histidine substitutions can alter a protein's affinity to bind nucleic acids and are shown to grant pH-dependent activity to transcription factors in cancer (41), we hypothesize that the activity of Rho^{R109H} exhibits a similar pH dependence that serves as a plastic adaptation to the neutral/alkaline fluctuations experienced during repeated starvation in LB broth. Using a combination of in vitro biochemical assays, fluorescence microscopy, and competitive coculture, we examined how *rho* R109H and $\Delta ydcl$ mutations contribute to the physiological adaptation of *E. coli* during repeated starvation. Additionally, through bioinformatic approaches, we further identify *rho* R109H alleles in wild bacterial strains that regularly experience neutral/alkaline fluctuations and infer amino acid residues of structural and functional importance within YdcI.

Results

Extensive Parallel Mutation in *rho* and *ydcl* During RLTS. To gain insight into how microbes adapt to recurrent nutrient resource fluctuations following prolonged periods of famine, we evolved 16 *E. coli* populations in parallel to a RLTS regime of 100-d feast/famine cycles for a total of 900 d (64). Every 100 d, we transferred 1 mL of the aged culture into 9 mL of fresh LB-Miller broth, replenishing each culture's resources. At this time, pretransfer aliquots of the populations were frozen to maintain a historical record of the evolution experiment. Growth in LB broth is supported through the catabolism of amino acids and leads to alkalinization of the medium within 24 h which remains between pH 8 and pH 9 until additional resources are provided (21, 22, 66). As such, *E. coli* cultures are subjected to resource-depleted, alkaline conditions for the vast majority of the RLTS regime, essentially 99 d (*SI Appendix, Fig. S1A*). Every 100 d, when cultures are replenished with resources, the medium pH decreases dramatically from approximately pH 9 to pH 7, before slowly returning to an alkaline pH over the next 24 h. Thus, populations adapted to these conditions must not only survive extended starvation under alkaline conditions but also cope with the sudden downward shift in pH and repletion of resources concurrently.

Metagenomic sequencing throughout the 900-d experiment revealed that approximately half (7/16) of the populations evolved fixed mutations in *rho*, which encodes the Rho-dependent transcription termination factor (Fig. 1A and SI Appendix, Fig. S2A). The majority of *rho* mutations (5/7) occurred in the first half of the RLTS experiment and swept to fixation within the first 400 d (Fig. 1B). By 700 d, *rho* mutations were fixed in a total of seven populations after which time no additional *rho* mutations were detected in the remaining nine populations. All identified *rho* mutations occur within the primary RNA-binding site of Rho. Thus, we suspect these mutations are likely to perturb interactions

between Rho and its RNA target (Fig. 1C and E and SI Appendix, Fig. S3). Furthermore, all five *rho* mutations that are fixed within the first 400 d result in an R109H nonsynonymous substitution, suggesting it may contribute to adaptation in RLTS conditions. After reconstructing the *rho* R109H allele into experimental ancestor background, we found that the R109H allele did not confer any considerable growth effects in conditions that previously produced other experimentally evolved *rho* mutations, including heat stress (56), exposure to ethanol (61), and osmotic stress (67) (SI Appendix, Fig. S4). This lack of phenotype is consistent with Rho's role as a pleiotropic "master-regulator" (68) and indicates

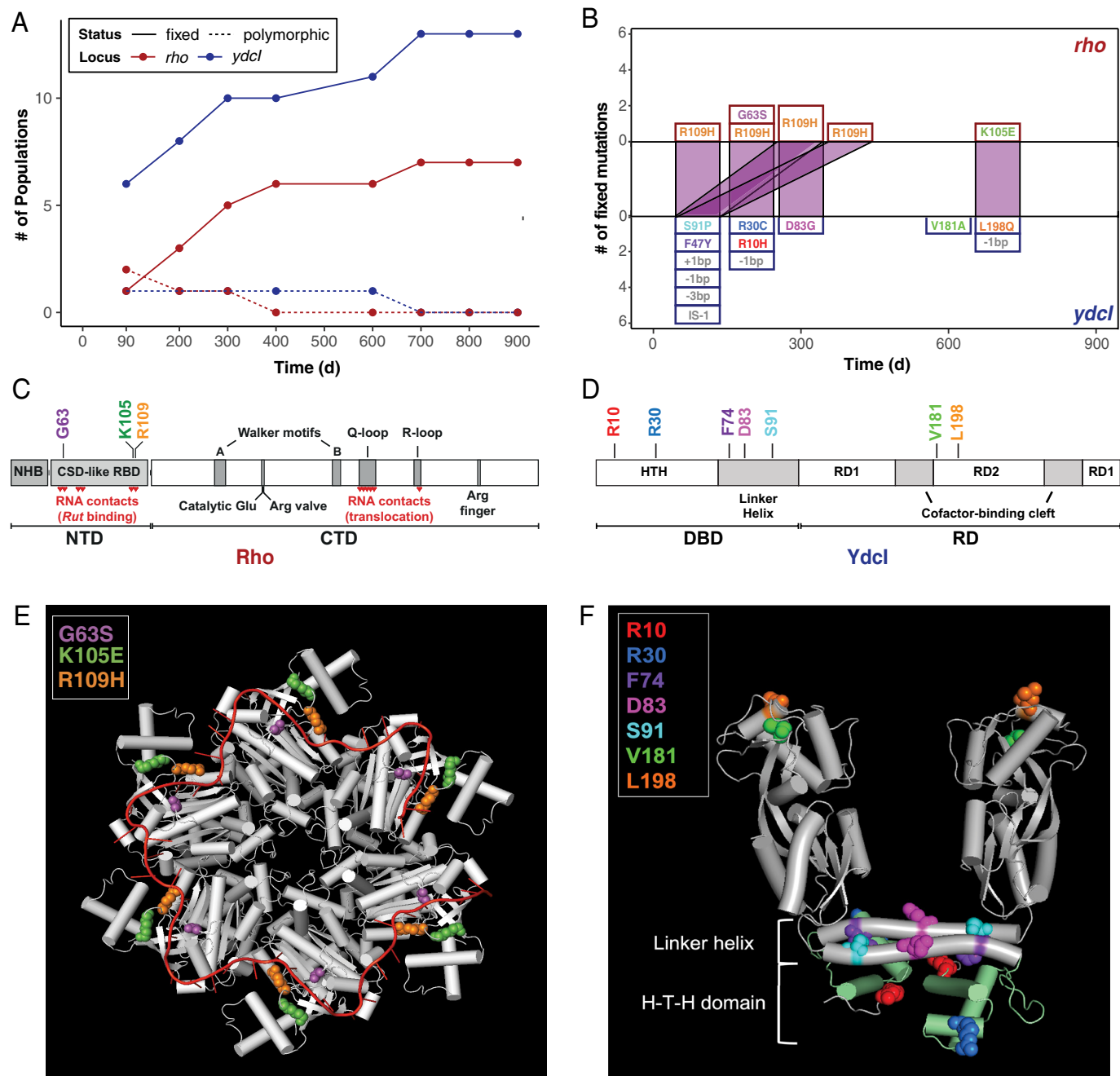


Fig. 1. RLTS selects for mutations in *rho* and *ydcl*. (A) Number of populations containing polymorphic (dashed line) or fixed (solid line) mutations in the *rho* (red) or *ydcl* (blue) loci over 900 d of evolution to RLTS conditions. (B) Number of fixed mutations in *rho* (top half) and *ydcl* (bottom half) genes indicating the timing at which each particular mutation arose over 900 d. Purple lines indicate alleles co-occurring within populations. The genetic location of affected (C) *rho* (orange: R109H, purple: G63S, green: K105E) and (D) *ydcl* residues (red: R10H, blue: R30C, purple: F74Y, magenta: D83G, cyan: S91P, green: V181A, orange: L198Q) and (E) structural locations of affected *rho* and (F) *ydcl* residues identified in populations over 900 d of evolution to RLTS conditions. Only the A and B chains of the Ydcl homotetramer are visualized for simplicity. Structural locations colored in green indicate H-T-H domain residues. NTD: N-terminal domain, CTD: C-terminal domain, NHB: N-terminal helix bundle, CSD: cold shock domain, RBD: RNA-binding domain, DBD: DNA-binding domain, RD: regulatory domain, HTH: helix-turn-helix.

that any phenotypes associated with the *rho* R109H allele may be contingent on specific conditions that occur during RTLS or dependent on an earlier arising mutation.

Since prior investigations implicate the evolution of arginine to histidine substitutions as a response to pH (40, 41, 69, 70), and histidine residues can serve as pH sensors (39, 71, 72), we refocused our investigation to include genes shaped by positive selection during RTLS and associated with pH homeostasis. We found that all populations with mutant *rho* alleles also contain mutations in the recently annotated *ydcI* gene, which encodes a LysR-type transcriptional regulator reported to affect the expression of around 60 genes in *E. coli*, some of which are associated with the pH response (65, 73) (Fig. 1 A and B and *SI Appendix, Fig. S2B*). Mutations in *ydcI* are pervasive and evolved in the vast majority (13/16) of RTLS populations (*SI Appendix, Table S1*). In each of these cases, the *ydcI* mutation arose simultaneously or before the *rho* mutation, suggesting that mutations in *ydcI* may be necessary for the fixation of mutations in *rho*.

In contrast to the localized mutations identified in *rho*, the mutations in *ydcI* are diverse, ranging from putative loss of function mutations—caused by IS-element insertions and small indels—to nonsynonymous SNPs whose functional consequences on YdcI activity are currently unknown (Fig. 1D). Nonsynonymous mutations in *ydcI* tend to cluster into three general genic regions. Using previous structural data for LysR-type proteins and the AlphaFold predicted structure for YdcI, we mapped the locations of these mutations to specific domains to gain insight into their potential functional impact (Fig. 1F). The affected residues R10

and R30 are found in the predicted helix–turn–helix domain and could lead to an abolishment of DNA-binding activity. Residues F74, D83, and S91 are all found in the $\alpha 4$ linker helix, and residues V181 and L198 are present in the junction between the two regulatory domains, regions that are critical to dimerization and effector binding, respectively, in well-studied LysR-type proteins (74). Together, this suggests that mutations resulting in loss or attenuation of YdcI function are under positive selection in RLTS conditions, and disruption of YdcI function may be necessary for the *rho* R109H allele to be beneficial.

Rho^{R109H} Mutants Display a pH-Sensitive In Vitro Phenotype.

Previous investigations have identified arginine to histidine substitutions that alter protein functionality in alkaline conditions (41, 70). Thus, we hypothesized that the activity of Rho^{R109H} may differ from that of WT Rho (Rho⁺) under alkaline conditions. To this end, we performed in vitro assays evaluating the capability of Rho to function as a helicase, terminate transcription, and bind RNA in neutral (pH 7) and alkaline (pH 9) conditions (Fig. 2 and *SI Appendix, Fig. S5*). At pH 7, we found no significant differences in the helicase activity (*t* test; $P = 0.829$) or transcription termination patterns of Rho^{R109H} and only modest differences in RNA affinity (*t* test, $P = 0.033$) compared to Rho⁺. By contrast, at pH 9, Rho^{R109H} exhibits significant reductions in its helicase activity (*t* test; $P = 5.54 \times 10^{-5}$), a complete inability to terminate transcription, and a significant decline in RNA affinity (*t* test, $P = 0.003$), while Rho⁺ remained functional. Moreover, Rho⁺ binding to RNA is largely unaffected by the change in pH conditions (*t* test,

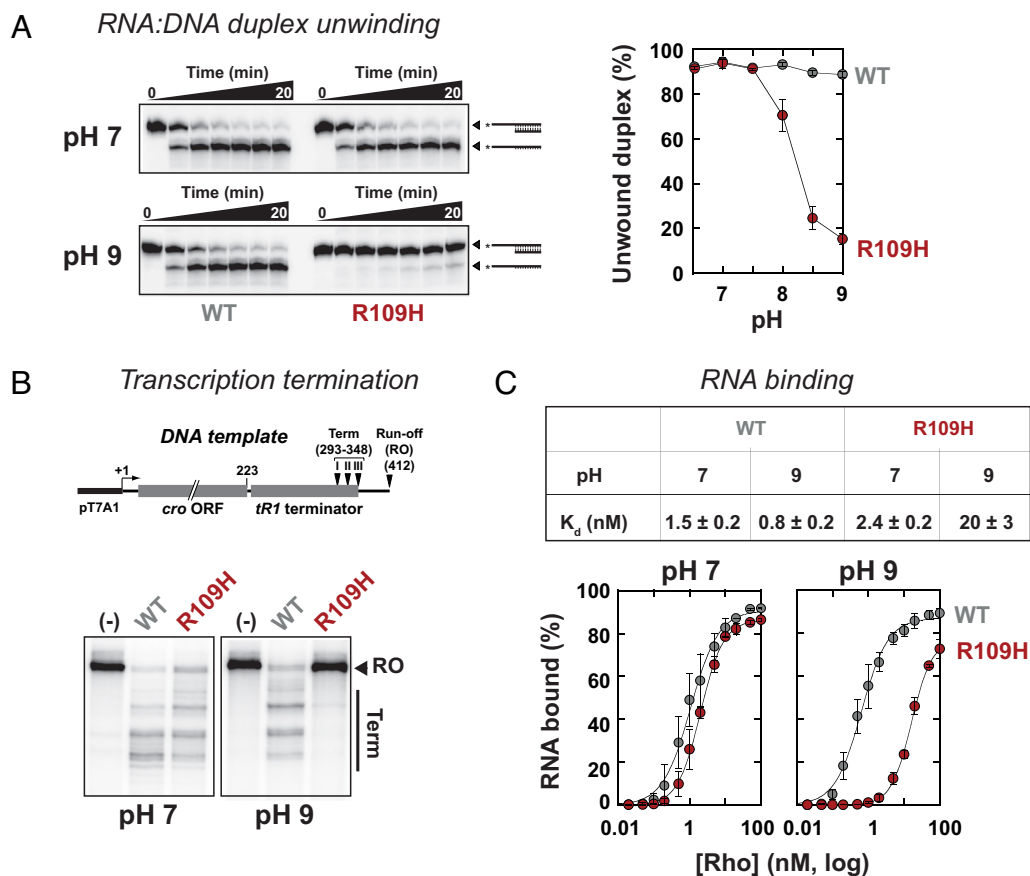


Fig. 2. The in vitro Rho assay reveals diminished activity of Rho^{R109H} at pH 9. The in vitro activities of Rho⁺ (WT) and Rho^{R109H} (R109H) were assessed at pH 7 and pH 9 in three ways: (A) efficiency of ATP-dependent unwinding of a RNA:DNA duplex containing a 5'-single-stranded *rut* overhang (graph: helicase activity after 20 min), (B) ability to terminate transcription at the λ tR1 terminator, and (C) ability to bind to RNA. A schematic of the DNA template used in the transcription termination assay is shown above gel images in (B). Chart above plots in (C) contains the calculated average K_d for WT and R109H proteins. Additional information regarding binding parameters can be found in Table 1.

Table 1. Equilibrium binding parameters for Rho-RNA complexes

Parameters*	WT		R109H	
	pH 7	pH 9	pH 7	pH 9
n	1.2 ± 0.2	1.3 ± 0.2	1.6 ± 0.2	1.7 ± 0.2
K _d (nM)	1.5 ± 0.2	0.8 ± 0.2	2.4 ± 0.2	20 ± 3

*Binding parameters were determined by nonlinear least-squares fit of the slot-blot data to the Hill equation: $F_b = F_{max}[\text{Rho}]^n / ([\text{Rho}]^n + K_d^n)$, where F_{max} is the maximal fraction of Rho-RNA complexes, K_d is the dissociation constant, and n is the Hill parameter reflecting binding cooperativity.

$P = 0.068$), while there is a significant reduction in Rho^{R109H} RNA binding as pH increases (t test, $P = 0.004$). These data collectively demonstrate that the activity of the Rho^{R109H} mutant is similar to the WT protein under neutral conditions, but is strongly reduced under alkaline conditions due, in part, to compromised RNA binding.

Of the transcripts where termination is Rho dependent, a fraction of termination events require an additional transcription-termination factor, NusG (47, 49), such as transcription termination that represses toxic prophage genes (46). These NusG-stimulated terminators have been shown to contain distinct *rut* features (47, 49) and are less sensitive to two disruptive primary binding site mutations, Rho^{F62S} and Rho^{Y80C}, than canonical terminators (75). To test the possibility that the R109H mutation may differentially impact the two classes of terminators, we conducted in vitro transcription experiments with two DNA templates encoding the NusG-stimulated terminators located within *aspS* and *yaiC* (49). With Rho⁺, termination at the *aspS* and *yaiC* sites is strongly stimulated by NusG at both pH 7 and pH 9 (SI Appendix, Fig. S6). Termination with the Rho^{R109H} mutant is also stimulated by NusG at pH 7, albeit to a lesser extent than Rho⁺. At pH 9, however, Rho^{R109H} can no longer trigger termination at the *aspS* and *yaiC* sites, even in the presence of NusG. These data indicate that pH regulates the activity of the Rho^{R109H} mutant at both NusG-stimulated and canonical Rho-dependent terminators (Fig. 2B).

Cells Containing *rho* R109H/ $\Delta ydcI$ Alleles Have an Altered Intracellular pH Response. The finding that Rho^{R109H} displays altered activity under alkaline conditions implies there must be changes in intracellular pH (pHi) to reveal the pH-dependent phenotype. To ascertain whether the introduction of the *rho* R109H and/or $\Delta ydcI$ alleles results in an alteration of pHi homeostasis, we measured pHi across a range of pH-adjusted buffers (pH 6.92 to 9.59) by staining cells with BCECF-AM (76–79) and compared their pHi response to that of WT cells. As the intensity of the fluorescent signal emitted from BCECF-stained cells depends on pH (78), we quantified the pHi of single cells with fluorescent microscopy.

Across the environmental pH conditions, WT and *rho* R109H single-mutant cells exhibited similar pHi values with a fitted range from 6.7 to 9.05 and 7.04 to 8.96, respectively (Fig. 3 and SI Appendix, Figs. S8 and S9). Alternatively, cells containing a single $\Delta ydcI$ mutation showed a reduced pHi range of 7.48 to 8.92, as $\Delta ydcI$ cells maintain a higher pHi than WT cells in acidic and neutral conditions (Fig. 3 and SI Appendix, Fig. S10). This effect is amplified in the double mutant *rho* R109H/ $\Delta ydcI$ cells which exhibit a pHi range of 7.53 to 9.67, maintaining a significantly elevated pHi across the entire range of environmental pH conditions compared to the WT (sign test; $n = 8$; $P = 0.008$) (Fig. 3C and SI Appendix, Fig. S11). Because pHi elevation in neutral conditions is only realized in mutant backgrounds containing $\Delta ydcI$, it is likely that double mutant *rho* R109H/ $\Delta ydcI$ cells constantly maintain an intracellular pH environment that

continuously manifests the pH-sensitive Rho termination activity via reduced RNA binding.

Benefits of *rho* R109H and $\Delta ydcI$ Alleles Vary in RLTS Environment. Considering the frequent co-occurrence of the *rho* R109H and $\Delta ydcI$ alleles in evolved populations and the necessity of both alleles for a significant alteration in pHi response, we hypothesized that the benefit of carrying the *rho* R109H allele could only be present in a $\Delta ydcI$ background. To address this, we “replayed” one cycle of the RLTS regime by growing cultures from different starting genotypes (WT, *rho* R109H, $\Delta ydcI$) for 100 d and sequenced the *rho* and *ydcI* loci from the aged cultures (Fig. 4A and SI Appendix, Fig. S12). We found that when starting from a *rho* R109H genotype, 8/12 populations evolved putative $\Delta ydcI$ mutations which swept to fixation within 100 d. Alternatively, when starting from a $\Delta ydcI$ genotype, only 3/12 populations evolved a *rho* R109H mutation, and only one of these *rho* R109H mutations had fixed. Importantly, when starting from a WT genotype, we did not observe the emergence of the *rho* R109H allele in a population without also detecting a fixed mutation in *ydcI*. Thus, *ydcI* loss-of-function mutations are recurrent in RLTS conditions and the appearance of the *rho* R109H mutation is unlikely to occur without a prior mutation in the *ydcI* gene.

Identifying the precise conditions under which each allele confers an advantage poses a challenge due to the continual evolution of the strains and the rapid accumulation of mutations as cultures age. While this is evident after “replaying” the evolution experiment, it may also account for the lack of significant differences in population cell density between strains over 100 d (SI Appendix, Fig. S1B). Consequently, we opted to conduct relevant phenotyping experiments over shorter periods to minimize any confounding effects potentially associated with the strains’ evolution. To mimic conditions experienced by populations during the RLTS regime, we performed pairwise competitions between each mutant and the WT ancestor in unbuffered, buffered pH 9, and buffered pH 7 LB medium for 1 and 14 d (Fig. 4B). When competing the WT ancestor against the *rho* R109H strain, we observe an early benefit to carrying the mutant *rho* allele after the first day of coculture, particularly in the pH 9 medium. However, after 14 d of coculture the WT ancestor strongly outcompetes the *rho* R109H strain in the unbuffered, buffered pH 9, and buffered pH 7 media. In contrast to *rho* R109H, $\Delta ydcI$ appears to exhibit considerably greater selection rates across the 14 d as the $\Delta ydcI$ strain outcompetes the WT ancestor at both time points and in all of the tested conditions. Notably, when the *rho* R109H allele is present in a $\Delta ydcI$ background, we no longer observe highly negative selection rates after 14 d. Instead, the double *rho* R109H/ $\Delta ydcI$ mutant strain outcompetes the WT strain under the unbuffered and buffered pH 9 conditions and maintains a high selection rate throughout the experiment, while in unbuffered pH 7 conditions it is neutral in coculture with the ancestor. These results indicate that the *rho* R109H allele is advantageous when resources are plentiful, especially in alkaline conditions, and disrupting the *ydcI* gene can mediate any tradeoffs associated with the *rho* R109H allele in resource-limited long-term stationary phase conditions.

In addition to assessing growth and survival in coculture, assessment of each strain in monoculture revealed no significant differences in the mutants’ survival over 14 d. The end of the stationary phase and subsequent onset of the death phase marks a considerable decline in population cell viability, which we consistently observe on day 3 of growth across all strains (80) (Fig. 4C and SI Appendix, Fig. S1B). Next, the transition into long-term stationary phase is characterized by a resurgence in population density

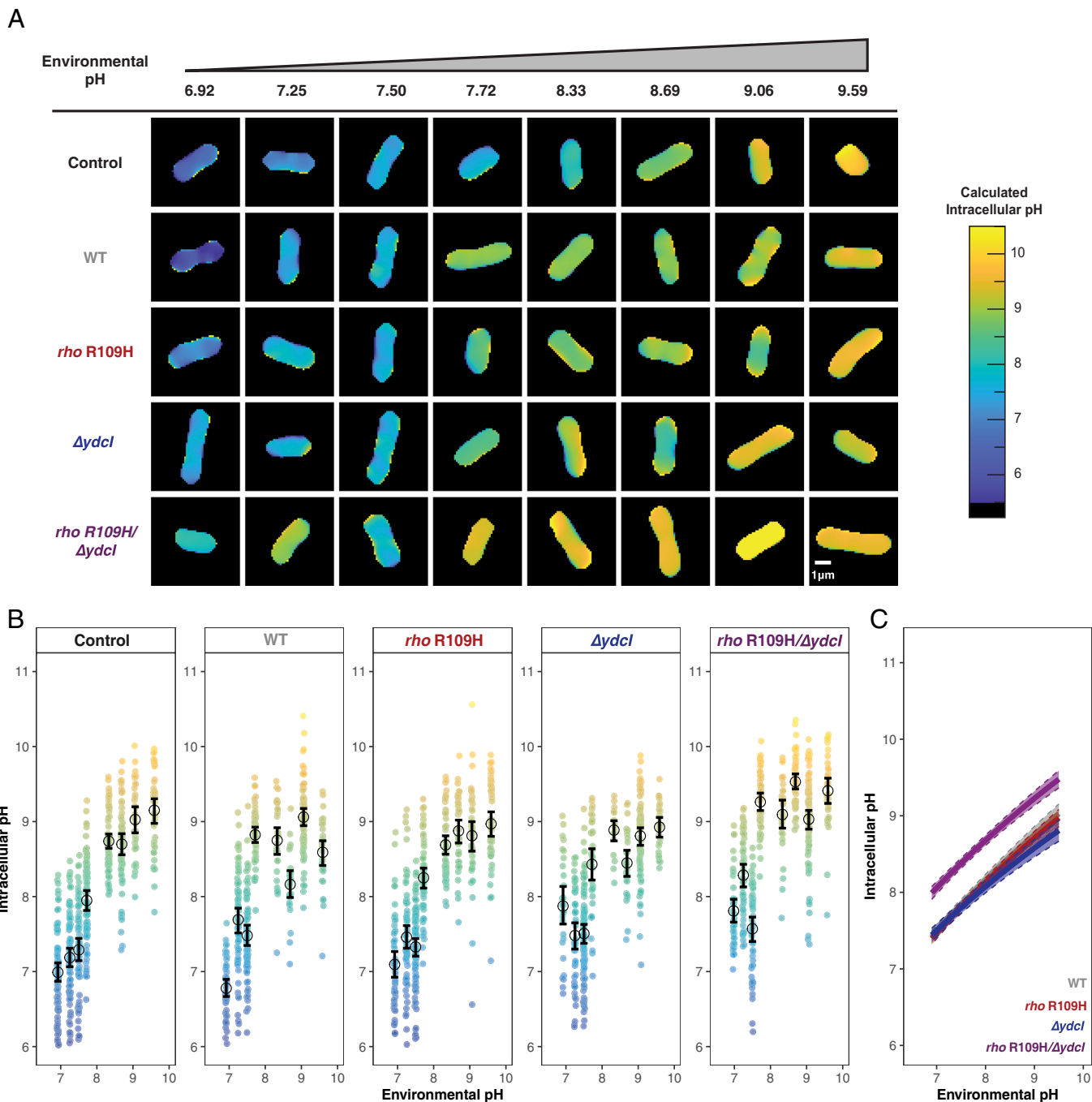


Fig. 3. *rho* R109H/ Δ *ydcI* cells have increased intracellular pH. The intracellular pH (pHi) of WT, *rho* R109H, Δ *ydcI*, and *rho* R109H/ Δ *ydcI* single cells was measured in buffers with increasing pH values. These measurements were derived from a ladder control (Control) containing WT cells treated with nigericin, yielding the pHi and environmental pH equal. (A) Representative microscopic images of single cells from tested strains in each pH buffered solution with colors of cells corresponding to their calculated pHi. Each image is cropped to $5.5 \times 5.5 \mu\text{m}$; a $1 \mu\text{m}$ scale bar is included in the bottom right image. The remaining microscopic images can be found in supplementary files. (B) pHi measurements derived from these images across the environmental pH conditions. Lightly shaded data points represent single-cell replicates with the color denoting the pHi. Error bars display 95% CI. (C) Plot displaying the pHi range of each strain in tested conditions using data from panel (B) illustrates an upward shift in the pHi range in the *rho* R109H/ Δ *ydcI* cells.

following the death phase, attributed to the substantial availability of dead cells providing resources for the surviving population (80). This resurgence in population cell density is highly repeatable, occurring on the 6th day of growth for the WT ancestor, *rho* R109H, and Δ *ydcI* strains (Fig. 4C). Notably, *rho* R109H/ Δ *ydcI* populations exhibit a resurgence a day earlier on day 5 of growth. This early population resurgence following the death phase highlights a unique advantage of *rho* R109H/ Δ *ydcI* as these cells can better utilize new resources as they become available, such as necromass and other metabolites released by dying cells.

Sequence Analysis Identifies *rho* R109H Alleles in Natural Isolates. Given the widespread presence of Rho across the bacterial domain and its essential role in many prokaryotes (81), we investigated the prevalence and distribution of a histidine residue at analogous positions within Rho (Fig. 5). Our initial search of the RefSeq database did not return any bacterial sequences with histidine at this location. However, a deeper search using PHI-BLAST identified several sequences from species isolated from diverse environments that harbor a histidine residue at positions analogous to the *E. coli* Rho R109. Many of these

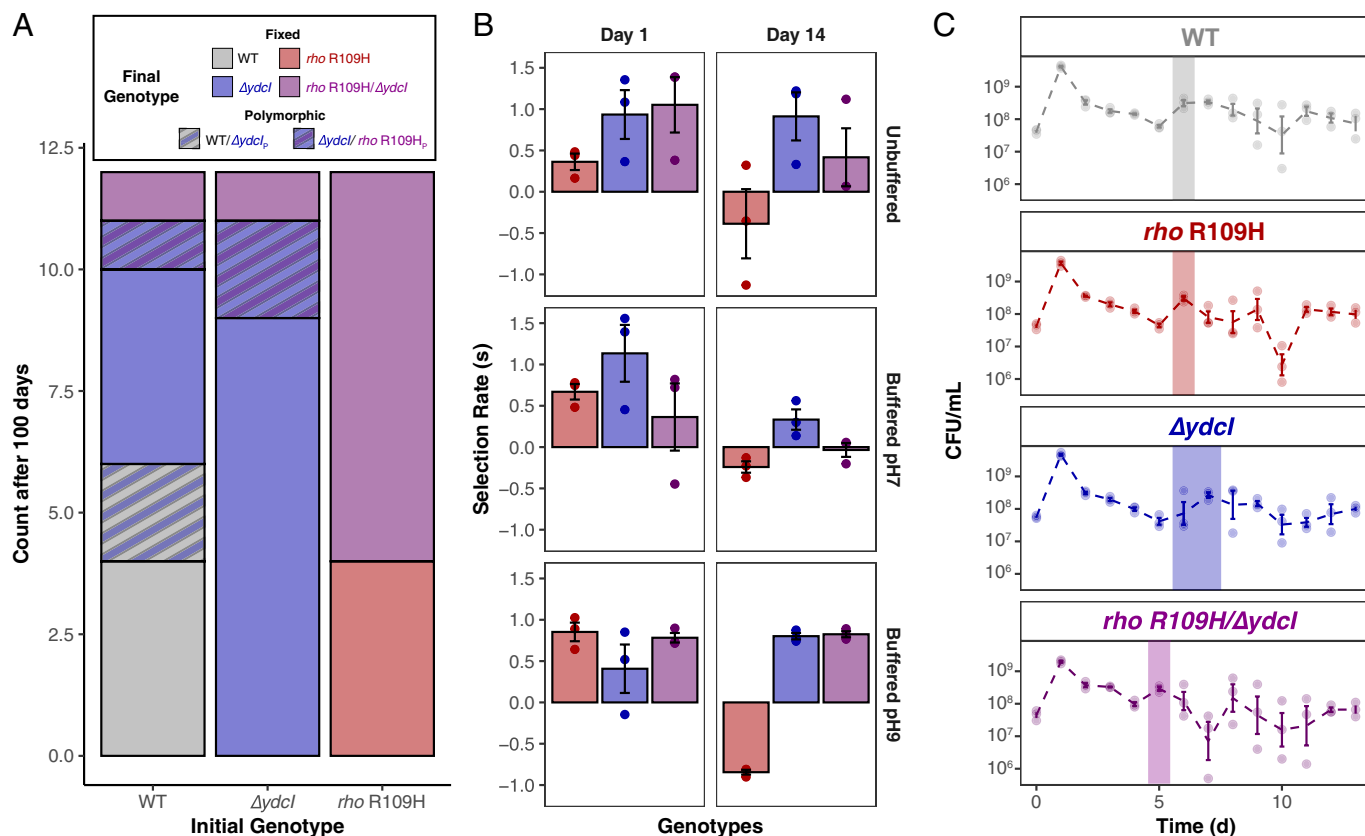


Fig. 4. Benefits of *rho* R109H and $\Delta ydcI$ alleles vary throughout the RLTS regime. (A) Frequency of final genotypes identified in populations after 12 replicate cultures of WT, $\Delta ydcI$, and *rho* R109H (initial genotypes) were grown in RLTS conditions for 100 d. A subscript of p denotes that the allele is polymorphic as indicated by the Sanger sequence. (B) Pairwise competitions between WT ancestor and mutant strains when cocultured for 1 or 14 d in unbuffered LB, LB buffered at pH 9, and LB buffered to pH 7. Colored bars indicate the median selection rate (s) for each mutant strain relative to the WT with single points representing each of three biological replicates. (C) Median CFU/mL of WT and mutant strains over 14 d of growth. Lightly shaded data points represent each of three biological replicates. Shaded vertical bars indicate the day of the first initial growth rebound postdeath phase. Error bars display 95% CI.

isolates originated from alkaline environments or those which fluctuate between alkaline and neutral conditions. The soil bacterium *Inquilinus limosus* was isolated from a region that reports alkalization of the soil (82, 83), while the *Poribacteria* genome was identified as part of a microbial mat in hypersaline, alkaline water (84, 85). The pathogen *Bartonella bacilliformis*, the causative agent of Carrion's disease, a neglected tropical disease, also encodes a histidine residue in Rho that may confer a pH-sensing phenotype as the pathogen alternates between neutral human blood and the alkaline midgut of sand flies (25, 86). The remaining species are isolated from aquatic environments with reported pH gradients. Planctomycetota was identified in sediment from the Auka marine hydrothermal vent (pH 6.5) in the Pacific Ocean (pH 8) (87), while Elusimicrobia was isolated from groundwater with a pH ranging from pH 6.5 to 8.5 (88, 89). Together, the absence of a histidine residue in the analogous position 109 of Rho in various lab-adapted bacterial reference strains, as well as the identification of Rho H109 residues in isolates that experience alkaline environments, is consistent with our results showcasing that this allele provides beneficial effects in alkaline environments.

Discussion

Here, we report an adaptive pH-sensing mutation in the global transcriptional terminator Rho (*rho* R109H) that emerged independently in multiple *E. coli* populations subjected to 900 d of RLTS conditions. In vitro analyses revealed a pronounced pH-dependent loss

of function, where Rho^{R109H} activity exhibited a sharp decline in the transition from neutral pH 7 to alkaline pH 9 conditions. This mutation was exclusively observed in strains that also contained a mutation in the transcriptional regulator gene *ydcI*, implying that in *E. coli* the *rho* R109H allele is beneficial in the RLTS environment when YdcI activity is attenuated or nonfunctional. Measurements of the pHi provide insight into the coexistence of these two alleles as we found that double mutant cells that carry both the *rho* R109H and $\Delta ydcI$ alleles exhibit a significantly more alkaline pHi, with respect to WT cells, across a spectrum of pH-adjusted solutions. These results imply that the intracellular environment of *rho* R109H/ $\Delta ydcI$ cells is conducive to conditions where Rho^{R109H} termination would be impaired. Pairwise competitions between the mutants and WT ancestor pinpoint distinct advantages of each allele in the RLTS environment. Results of these competitions suggest that the *rho* R109H allele is beneficial during nutrient resource repletion as this mutation alone confers a fitness benefit only when resources are abundant, with an enhanced fitness when grown in LB broth adjusted to pH 9. However, this advantage is transient, as by 14 d of coculture, the *rho* R109H allele is no longer beneficial by itself. Instead, we observed that the deletion of *ydcI* masks the detrimental effects of the *rho* R109H allele during resource-depleted conditions, illustrating that the elimination of YdcI function generates an intracellular environment that better tolerates the plasticity of the *rho* R109H allele. Collectively, these data reveal a nuanced interplay between both alleles as they jointly provide unique contributions to navigating the complex stresses inherent to RLTS.

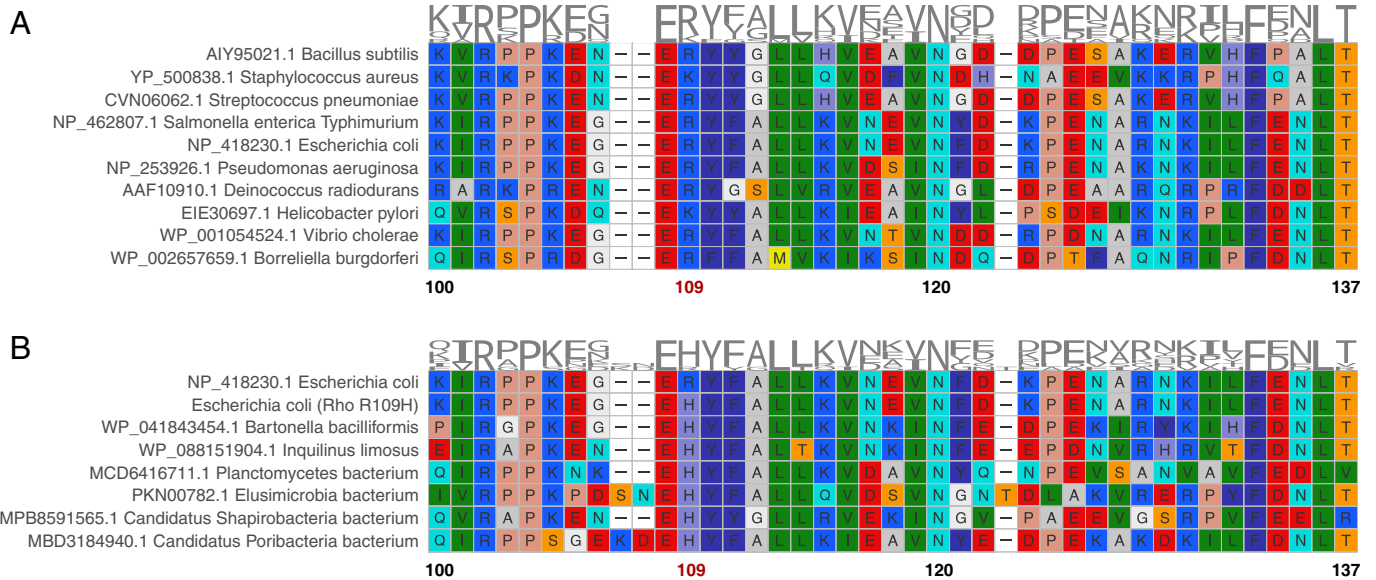


Fig. 5. Amino acid alignment of the Rho N-terminal RNA-binding domain in laboratory strains and natural isolates. Alignments of Rho sequences from selected (A). RefSeq genomes and the mutated R109H *E. coli* clone with natural (B) non-*E. coli* isolates that encode a Histidine residue at the analogous position. Natural non-*E. coli* isolates were identified with PSI-BLAST. For both alignments, NCBI accession numbers for the protein sequence are included on the y axis. Coordinates on the x-axis indicate analogous positions in *E. coli* Rho.

Prior research investigating the consequences of Rho impairment and the effects of various *rho* mutations on gene expression offers insight into the potential impacts of the *rho* R109H allele on resource utilization during pH fluctuations. In general, the impairment of Rho activity leads to an overall enrichment in transcripts due to transcriptional readthrough of Rho-dependent terminators (90). However, it appears that the identity and degree of differentially expressed genes vary based on the location and nature of the *rho* mutation, creating a challenge in pinpointing the exact benefit of the *rho* R109H allele. Although adaptive Rho mutations in residues that constitute the primary binding site are less common (91, 92), these mutants do appear to be less disruptive to gene expression and have less enrichment in prophage gene expression, compared to evaluated secondary binding site mutants, which could partially explain why the *rho* R109H mutation is not detrimental (46, 75). In some primary binding site mutants, a defect in RNA binding can be overcome at terminators with high NusG dependence (75). However, the Rho^{R109H} in vitro activity at two such terminators, *aspS* and *yaiC*, is also impaired in pH 9 conditions, signifying that the effects of this mutation vary from previously described primary binding site mutants. Adaptive mutations in *rho* can confer the ability to use novel substrates due to the upregulation of many metabolic pathways (60, 93). Rho has been demonstrated to play a role in the pH response as changes in Rho activity can alter pH homeostasis (94). Rho also controls the expression of genes related to the pH response (46), including tryptophanase, one of the most abundant proteins present in LB broth buffered to pH 9 (95). Adaptation to complex stresses elicits a distinct response that differs from the response to individual stresses (96). Thus, the pleiotropic nature of Rho may enable it to effectively navigate complex stress (68).

In contrast to our current understanding of Rho's function, very little is known about YdcI and its regulatory targets. What is understood is that *ydcI* is found across closely related enterobacterial genera including, *Escherichia*, *Salmonella*, *Citrobacter*, and *Klebsiella*, and its regulatory function has since diverged from its most characterized role in regulating acid-stress responses in *S. Typhimurium* to a more ambiguous role in mediating acid and alkaline stress in *E. coli* (73). While there are differing reports of

the loci regulated by *ydcI* in *E. coli*, there is agreement on its role in activating expression of the *rpoS* stabilization protein *iraP* (65, 73). Thus, while we currently do not know exactly which genes are differentially expressed due to the *rho* R109H/ $\Delta ydcI$ double mutation, it is likely that changes in gene expression induced by these mutations in alkaline conditions impact pH and other stress responses. Since we do not observe fixation of the *rho* R109H mutation in cells without a deletion of *ydcI*, it is possible that the combination of these two alleles may relieve any potential detrimental effects on gene expression induced by alteration of Rho activity, especially in the long-term stationary phase portion of the RLTS regime, and help to explain why YdcI function has to be eliminated in order for the *rho* R109H allele to be beneficial.

The necessity of a permissive mutation, such as the disruption of *ydcI*, is not unprecedented as adaptive nonsynonymous mutations in *rho* often do not confer immediate fitness advantages and typically necessitate additional mutations for the development of specific phenotypes (57, 60, 97). This occurrence is exemplified in the *rho* R109H mutant as its mutant state is likely not actualized unless the cellular environment is altered through the elimination of YdcI. Within *rho* R109H/ $\Delta ydcI$ cells, the elevated pH_i would likely result in a more uniform activity state for Rho since the majority of histidine residues would be deprotonated, effectively genetically assimilating the plastic *rho* R109H allele in its beneficial mutant state (98). Physiologically, the alkalized pH_i of *rho* R109H/ $\Delta ydcI$ cells would help alleviate stress associated with maintaining pH homeostasis in an alkalized environment. In these conditions, pH homeostasis is dependent on the activity of electrogenic antiporters, such as the NhaA Na⁺/H⁺ pump, to power proton entry, placing a large energetic burden on maintaining a proton motive force (24). Upstream of *nhaA* lies *sokC*, which contains a Rho-dependent terminator (47, 99). Thus, it is possible that when Rho activity is compromised, transcriptional readthrough from *sokC* leads to increased expression of *nhaA*. Moreover, by maintaining a pH_i that is more alkaline than the environment, *rho* R109H/ $\Delta ydcI$ cells would be less dependent on the activity of cation/proton antiporters to maintain homeostasis. This physiological benefit extends to the pH fluctuation period during resource replenishment when there is an abrupt downshift to a neutral

environmental pH. In this condition, our data indicate that *rho* R109H/ $\Delta ydcI$ cells would remain highly alkaline, leading to an even larger difference in protons across the membrane that would favor proton entry. Given that many metabolic substrates are often cotransported with H^+ via symporters, the increased ΔpH of *rho* R109H/ $\Delta ydcI$ cells would help to drive the import of resources (100). Thus, the alkalization of *rho* R109H/ $\Delta ydcI$ cells would not only help to reduce the energy required to maintain pH homeostasis but would also enable the ability to better capitalize on resources through more efficient transport of the available resources.

In summary, these data report a pH-sensitive mutation in an essential global regulator that confers significant physiological effects when paired with the inactivation of a mostly unknown transcription factor related to pH homeostasis. These mutations primarily evolve in the first 300 d of experimental evolution, illustrating how phenotypically plastic traits can facilitate rapid adaptation to complex, fluctuating environments. Despite the absence of this mutation from the current literature, we identify several natural isolates from fluctuating neutral/alkaline conditions carrying this allele, illustrating the power of experimental evolution for identifying functionally important mutations relevant to natural environments. Finally, the phenomenon described herein may signify genetic preassimilation via permissive mutations as a widespread adaptive mechanism for challenging complex environments. An emerging hallmark of cancer involves perturbations in pH_i that manifest similarly to *rho* R109H/ $\Delta ydcI$ cells, where the pH_i is maintained higher than that of the extracellular environment (101, 102). In cancers, these alterations can be induced through arginine to histidine mutations that confer pH-sensing capabilities, particularly in global regulators, subsequently altering gene expression and reshaping the cellular environment (40, 41). This suggests particular amino acid mutational signatures could yield effects applicable across all domains of life and that a greater understanding of how these patterns could contribute to changes in cellular physiology is of paramount importance.

Materials and Methods

Strain Construction and Growth Conditions. All bacterial strains originate from PFM2, a prototrophic derivative of *E. coli* MG1655 K-12 that was provided by Dr. Patricia Foster (Indiana University) (103). The *rho* R109H substitution was cloned into the PFM2 $\Delta araBAD$ background using the Church protocol (104). The $\Delta ydcI$ and *rho* R109H/ $\Delta ydcI$ mutants were generated by moving the *ydcI*723(del)::kan cassette from the Keio collection strain JW5226 (105) to the PFM2 WT and *rho* R109H strains, respectively, using P1 vir transduction (106). Mutations were confirmed via PCR and Sanger sequencing. The *rho* R109H mutation was confirmed using a forward primer sequence of 5'-GGTGATGGCGTACTGGAGAT-3' and a reverse primer sequence of 5'-GTGCCACAATCAGACCAGC-3'. For the *ydcI* locus, mutations were confirmed using the forward primer 5'-CGGCACGATTAAGTGGCCGT-3' and reverse primer 5'-CGCCGTGATGCTGCCCAA-3'.

Identification of Mutations in Time-Series Whole-Population Metagenomic Sequencing. Mutations in *rho* and *ydcI* were initially detected during the analysis of longitudinal metagenomic sequencing of 16 *E. coli* populations that were experimentally evolved in 100-d feast/famine cycle conditions (64). These populations originate from four different genetic backgrounds: PFM2; PFM2, $\Delta araBAD$; PFM2, $\Delta mutL$; or PFM2, $\Delta araBAD$, $\Delta mutL$. The deletion of the $\Delta araBAD$ locus serves as a neutral marker that enables the detection of cross-contamination between lines during experimental evolution by plating on TA agar (10 g/L tryptone, 1 g/L yeast extract, 5 g/L NaCl, 16 g/L agar, 10 g/L L-arabinose, and 0.005% tetrazolium chloride) (107), while the deletion of $\Delta mutL$ disrupts methyl-directed mismatch repair and allows for the examination of the evolutionary process in a mutator phenotype. The relevant genotypes of populations adapted to 100-d feast/famine cycles can be found in *SI Appendix, Table S1*.

Structural Analysis. The quaternary structure of YdcI was predicted with SWISS-MODEL from an alpha-fold predicted structure for YdcI (P77171) on UniprotKB. As YdcI is annotated as a LysR-family transcriptional regulator, which are typically homotetramers (108, 109), we focused our search on the homology options in the SWISS-MODEL repository that were homotetramers and based on OxyR—another member of the LysR family (templates: 4 x 6g.1.A and 6g1d.1.A). Residues that acquired nonsynonymous mutations throughout experimental evolution were highlighted in PyMol. For the structure of Rho, the most recent and most detailed cryoEM reconstruction of an *E. coli* Rho-RNA complex was used (#8E6W), while PyMol was used to highlight features of interest.

In Vitro Analysis of Rho Activity. Plasmid pET28bR109H for overexpression of the R109H mutant was obtained by site-directed mutagenesis of plasmid pET28bRho (kindly provided by Pr. James Berger, Johns Hopkins University) using the NEBuilder HiFi kit (New England Biolabs). The R109H mutant was overexpressed in BL21(DE3)pLysS cells carrying the pET28bR109H plasmid and purified as described for WT Rho (110).

Duplex unwinding experiments were performed as described (110) with minor modifications. Briefly, 5 nM RNA:DNA duplexes bearing a ^{32}P label and a *rut* site [substrate C (111)] was incubated for 5 min at 37 °C with 20 nM Rho hexamers in helicase buffer (150 mM potassium acetate and 20 mM of MES, HEPES, or EPPS at the indicated pH). Then, 1 mM $MgCl_2$, 1 mM ATP, and 400 nM Trap oligonucleotide (complementary to the DNA strand of the duplexes) were added to the reaction mixture before incubation at 30 °C. Reaction aliquots were withdrawn at various times, quenched with two volumes of quench buffer (20 mM EDTA, 0.5% SDS, 150 mM sodium acetate, and 4% Ficoll 400), and analyzed by 9% polyacrylamide gel electrophoresis (PAGE) and phosphorimaging (Typhoon FLA-9500 instrument and ImageQuant TL v8.1 software, Cytiva).

Transcription termination experiments were performed as described (112) with minor modifications. Briefly, DNA template encoding the λ tR1 terminator (0.1 pmol), *E. coli* RNA polymerase (0.4 pmol; New England Biolabs), Rho (1.4 pmol), and SUPERase-In (0.5 U/ μ L; Ambion) were mixed in 18 μ L of transcription buffer (150 mM potassium acetate, 5 mM $MgCl_2$, 1 mM DTT, 0.05 mg/mL BSA, and either 20 mM HEPES, pH 7.0, or EPPS, pH 9.0) and incubated for 10 min at 37 °C. Then, 2 μ L of initiation mix (2 mM ATP, GTP, and CTP, 0.2 mM UTP, 2.5 μ Ci/ μ L of ^{32}P -aUTP, and 250 μ g/mL rifampicin) were added to the mixtures before further incubation for 20 min at 37 °C. Reactions were quenched with 70 mM EDTA, 0.1 mg/mL tRNA, and 0.3 M sodium acetate, phenol extracted, concentrated by ethanol precipitation, and then analyzed by denaturing 8% PAGE and phosphorimaging.

Rho-RNA dissociation constants (K_d) were determined using a filter-binding assay, as described (113). Briefly, ~ 10 fmoles of ^{32}P -labeled RNA substrate (RNA strand from substrate C) were mixed with various amounts of Rho in 100 μ L of binding buffer (0.1 mM EDTA, 1 mM DTT, 150 mM potassium acetate, 20 μ g/mL BSA, and either 20 mM HEPES, pH 7.0, or 20 mM EPPS, pH 9.0). After incubation for 10 min at 37 °C, the samples were filtered through stacked [top] nitrocellulose (Amersham Protran) and [bottom] cationic nylon (Pall Biodyne B) membranes using a Bio-dot SF apparatus (Bio-Rad). The fractions of free and Rho-bound RNA (retained on the nylon and nitrocellulose membranes, respectively) as a function of Rho concentration (expressed in hexamers) were then determined by phosphorimaging of the membranes.

Quantification of Intracellular pH. Intracellular pH was determined using the pH-sensitive fluorescent dye BCECF-AM. In brief, the fluorescence of this dye depends on the environmental pH, with high pH environments showing increased levels of fluorescence. It is a ratiometric dye, meaning that we utilize the ratio of fluorescence emission (525 nm) when excited at two different wavelengths (470 nm and 440 nm). Because the relative intensities in these two channels depend on both the imaging conditions (light intensity, emission filters, exposure time, etc.) and the pH, the conversion from the ratio of intensities to pH units needs to be calibrated utilizing the same approach as the experimental collection. Here, we used the ionophore nigericin as a way to collapse the pH gradient between the inside of control cells and their external buffered environment. This allowed us to measure intensities ratios and build a conversion function from intensities to pH while the BCECF dye was still in the presence of cellular components.

Cultures of each experimental strain, including an additional WT culture used for calibration of ratiometric fluorescence calibration (control), were grown overnight in LB broth. Due to the significant autofluorescence exhibited by LB broth, it could not be utilized for this microscopy-based approach. To address this issue, we thoroughly washed and resuspended cells from the overnight cultures in Ringer's buffer, which is specifically formulated to minimize osmotic stress and commonly used to wash cells prior to staining and visualization on a microscope (114, 115). Specifically, a 1 mL aliquot from each culture was washed two times via centrifugation and resuspended in 500 μ L of unbuffered Ringer's buffer (1/4X) (Oxoid). We stained cells for 30 min at 37 $^{\circ}$ C with 2 μ M BCECF-AM (Invitrogen). In addition to BCECF-AM staining, we added 5 μ L of nigericin (Sigma Aldrich) to the tube containing the WT ladder standard to allow intracellular pH to equilibrate with the external environment. Following staining, we performed two additional washes via centrifugation using 500 μ L of unbuffered 1/4X Ringer's solution (Oxoid). 100 μ L aliquots of each experimental strain and the ladder sample were transferred into five separate tubes. We centrifuged each tube for 1 min at 13,000 \times *g* and resuspended the pellets in one of seven 1/4X buffered Ringer's solutions (pH 6.92, 7.25, 7.72, 8.33, 8.69, 9.06, and 9.59). We prepared buffered Ringer's solutions using 50 mM of 1,3-Bis[tris(hydroxymethyl)amino]propane (Acros Organics) and adjusted the pH to the appropriate level using 1 M HCl. Once resuspended into pH-adjusted solutions, we imaged cells after approximately 30 min.

For each condition, 7 μ L of cells was sandwiched between a 22 mm square #1.5 coverslip and a standard glass slide, providing sufficient fluid volume for cells to remain in solution but in approximately the same focal plane of the microscope. Cells were imaged on a Nikon Ti inverted microscope (Nikon Instruments, Melville, NY) equipped with an Andor Zyla sCMOS camera (Oxford Instruments, Abingdon, Oxfordshire), Spectra/Aura light engine (Lumencor, Beaverton, OR), and an Apo TIRF 60X Oil DIC N2 NA 1.49 objective (Nikon Instruments, Melville, NY). The BCECF fluorescence intensity was imaged in two channels (1: Ex 470 nm, Em 525/50 nm, and 2: Ex 440 nm, Em 525/50 nm). We used a semiautomated MATLAB script (MathWorks, Natwick, MA) to segment cells and quantify the fluorescence intensity. In brief, the process of segmentation identifies which pixels in the image correspond to individual objects or regions. Within each of these regions, the total intensity from each fluorescence channel was computed. Regions around these cells were used as proxies for the local background intensity and subtracted from the total intensity in each region. From these background subtracted intensities, the intensity ratio was calculated. To assist in the automation of this process, we utilized standard approaches in image processing which are described below. Images underwent a spatial bandpass filter (spatial frequencies between 220 nm and 1,100 nm) to remove salt and pepper noise and background intensity. Objects were then segmented as individual regions if above a certain intensity threshold. Because cells were plated at a sufficiently low density to ensure single objects, a relative threshold for each image was set as the intensity such that approximately the top 1,000 pixel values were above the threshold (quantile of 0.9998). To ensure that the entire region of each cell was included, and to deal with the fact that these two imaging channels have a small spatial shift from one channel to the other, these regions were then dilated by disks of radius 2 μ m. Background regions were defined by dilating these regions by a further 2 μ m, and removing the objects from these masks, yielding regions that are near, but not overlapping with, individual objects. The intensity for each object in each channel was determined as the background-subtracted sum of all the pixels in each region. Lists of relative intensities of these objects were then imported into RStudio. Samples treated with nigericin were used to determine the coefficients A and B in a fit of $\text{pH}_{\text{obs}} = A \cdot \log(\text{intensityRatio}) + B$.

To statistically determine differences in intracellular pH across the WT and engineered mutant strains, we fit the relationship between intracellular pH and environmental pH to a logarithmic function [$\text{Intracellular pH} \sim a \cdot \log(\text{Environmental pH}) + k$] using a nonlinear least squares method in the R package "nlm." The fit was calculated across the measured interval of pH 7 to 9.5, and CI were calculated via uncertainty propagation with the function predictNLS which calculates CI for the fitted values of nonlinear models by using first-/second-order Taylor expansion and Monte Carlo simulation.

Replaying of RLTS Regime. To determine the prevalence of the *rho* R109H and $\Delta ydcI$ alleles in the RLTS condition and to parse out any patterns in their co-occurrence, we replayed one cycle of the RLTS regime by incubating WT, *rho*

R109H, and $\Delta ydcI$ cultures for 100 d after which time we examined the *rho* and *ydcI* loci for acquired mutations. We inoculated 12 cultures of WT, *rho* R109H, and $\Delta ydcI$ strains in 10 mL of LB broth each originating from a separate colony from an LB agar plate freshly prepared from frozen glycerol stocks. We cultivated each culture at 37 $^{\circ}$ C and shaken upright at 180 rpm for a total of 100 d. We left cultures undisturbed during this time except for a brief period every 10 d when the culture tubes were gently removed from the incubator and added sterile deionized water to achieve a volume of 10 mL to counteract evaporation. After 100 d, we removed the cultures and centrifuged them 2,500 \times *g* for 10 min. We froze the resulting pellet of bacterial biomass in liquid nitrogen and it was stored at -80° C until DNA extraction was performed. We extracted DNA from the pellets using a DNeasy UltraClean Microbial Kit (Qiagen) and used the resulting DNA samples as template for PCR. We performed PCR using the same primers previously mentioned that were used for confirmation of the initial mutation. The PCR products were purified using the Monarch PCR & DNA Cleanup Kit (NEB) and sent for Sanger sequencing (GENEWIZ).

Pairwise Competition Assays. To determine the fitness outcomes of the mutant strains relative to the WT ancestral strain, we performed pairwise competition assays (107, 116). Here, culture tubes containing a 50:50 starting proportion of two competing strains are grown for a given period, at which time they are sampled to determine the resulting proportions of each strain following growth. Each competing strain contains either an intact *araBAD* operon or $\Delta araBAD$ genotype and can be differentiated from each other by plating on TA agar (10 g/L tryptone, 1 g/L yeast extract, 5 g/L NaCl, 16 g/L agar, 10 g/L L-arabinose, 0.005% tetrazolium chloride) where the WT *araBAD* strain produces light pink colonies and the $\Delta araBAD$ strain produces bright red colonies. Overnight cultures were prepared for each strain using colonies picked from freshly streaked LB agar plates obtained from frozen stocks. For each competition, we inoculated 10 mL of LB broth with 50 μ L of overnight culture from both competitors. We set up individual competitions for each sampling time point, as vortexing and resampling of the same competition tube has been shown to alter fitness outcomes (23). Before incubation, we sampled each competition to determine precise starting proportions by collecting a 100 μ L aliquot, serially diluting in PBS, and plating on TA agar. All competition tubes were incubated at 37 $^{\circ}$ C until the sampling time point at which time a 100 μ L sample was removed, serially diluted in PBS, and plated on TA agar. All TA agar plates were incubated at 37 $^{\circ}$ C for 24 h before colonies were enumerated. For competitions using buffered media, we added 50 mM 1,3-Bis[tris(hydroxymethyl)amino]propane (Acros Organics) and adjusted the pH to either 7.0 or 9.0 using 1 M HCl.

Survival Assays. We assessed the survival of our strains by monitoring their population density over the course of 14 d. We inoculated three replicate overnight cultures of WT, *rho* R109H, $\Delta ydcI$, and *rho* R109H/ $\Delta ydcI$ strains in 10 mL of LB broth each originating from a separate colony from an LB agar plate freshly prepared from frozen glycerol stocks and incubated them for 18 h at 37 $^{\circ}$ C. The survival assay was initiated by aliquoting 100 μ L of each overnight culture into 14 individual culture tubes filled with 10 mL of fresh LB broth. We incubated each culture at 37 $^{\circ}$ C, shaken upright at 180 rpm until the appropriate sampling time point. We set up individual cultures for each sampling time point, as vortexing and resampling of the same culture tube has been shown to alter fitness outcomes (23). Every 24 h, the culture tube corresponding to the sampling time point was removed from the incubator and gently vortexed. We then removed 100 μ L from the culture and performed serial dilutions in PBS. We plated 100 μ L aliquots of the dilutions on LB agar plates and enumerated the colonies from countable plates after 24 h of incubation at 37 $^{\circ}$ C.

Identification of Other Bacterial *rho* R109H Alleles. Rho homologs containing a histidine at the analogous *E. coli* R109 residue were identified using blastp with the Pattern Hit Initiated (PHI-BLAST) algorithm (117). The following PHI pattern EH[YF][YFG][AGS][LM][LVT] targets R109H substitutions to the conserved ERFYALL motif from the *E. coli* Rho sequence (NP_418230.1) while allowing for any variation observed after alignment to Rho sequences with COBALT (118) across nine additional species of bacteria spanning the bacterial tree of life: *Bacillus subtilis* (AIY95021.1); *Borrelia burgdorferi* (WP_002657659.1); *Deinococcus radiodurans* (AAF10910.1); *Helicobacter pylori* (EIE30697.1); *Pseudomonas aeruginosa* (NP_253926.1); *Salmonella enterica* typhimurium (NP_462807.1); *Staphylococcus aureus* (YP_500838.1); *Streptococcus pneumoniae* (CVN06062.1); and *Vibrio cholerae* (WP_001054524.1) (Fig. 5).

Data, Materials, and Software Availability. All raw data and code needed to reproduce the figures in this study are available at https://github.com/BehringerLab/Rho_Ydcl_pH. All other data are included in the manuscript and/or *SI Appendix*. Previously published data were used for this work (18).

ACKNOWLEDGMENTS. We would like to thank the Advanced Computing Center for Research and Education at Vanderbilt and Vanderbilt Cell Imaging Shared Resource (supported by NIH Grants CA68485, DK20593, DK58404, DK59637, and EY08126), specifically the Nikon Multi-Excitation TIRF Microscope acquired under S10-OD018075-01A1. This work was supported by Army Research Office Grant W911NF-21-1-0161 (M.G.B.), NIH Grant R35GM150625 (M.G.B.), and French Agence Nationale de la Recherche Grant ANR-19-CE44-0009-01 (M.B.)

1. A. Aertsens, C. W. Michiels, Stress and how bacteria cope with death and survival. *Crit. Rev. Microbiol.* **30**, 263-273 (2004).
2. G. Lambert, E. Kussell, Memory and fitness optimization of bacteria under fluctuating environments. *PLoS Genet.* **10**, e1004556 (2014).
3. J. Nguyen, J. Lara-Gutiérrez, R. Stocker, Environmental fluctuations and their effects on microbial communities, populations and individuals. *FEMS Microbiol. Rev.* **45**, fuaa068 (2021).
4. R. Y. Morita, Bioavailability of energy and its relationship to growth and starvation survival in nature. *Can. J. Microbiol.* **34**, 436-441 (1988).
5. A. T. Reese *et al.*, Microbial nitrogen limitation in the mammalian large intestine. *Nat. Microbiol.* **3**, 1441-1450 (2018).
6. J. Hobbie, E. Hobbie, Microbes in nature are limited by carbon and energy: The starving-survival lifestyle in soil and consequences for estimating microbial rates. *Front. Microbiol.* **4**, 324 (2013).
7. R. Kolter, D. A. Siegel, A. Tormo, The stationary phase of the bacterial life cycle. *Annu. Rev. Microbiol.* **47**, 855-874 (1993).
8. M. M. Zambrano, D. A. Siegel, M. Almirón, A. Tormo, R. Kolter, Microbial competition: *Escherichia coli* mutants that take over stationary phase cultures. *Science* **259**, 1757-1760 (1993).
9. M. M. Zambrano, R. Kolter, GASping for life in stationary phase. *Cell* **86**, 181-184 (1996).
10. S. E. Finkel, Long-term survival during stationary phase: Evolution and the GASP phenotype. *Nat Rev Microbiol* **4**, 113-120 (2006).
11. S. Katz *et al.*, Dynamics of adaptation during three years of evolution under long-term stationary phase. *Mol. Biol. Evol.* **38**, 2778-2790 (2021).
12. N. R. Ratib, F. Seidl, I. M. Ehrenreich, S. E. Finkel, Evolution in long-term stationary-phase batch culture: Emergence of divergent *Escherichia coli* lineages over 1,200 days. *mBio* **12**, e03337-20 (2021).
13. W. R. Shoemaker *et al.*, Microbial population dynamics and evolutionary outcomes under extreme energy limitation. *Proc. Natl. Acad. Sci. U.S.A.* **118**, e2101691118 (2021).
14. T. Aouizerat *et al.*, Eukaryotic adaptation to years-long starvation resembles that of bacteria. *iScience* **19**, 545-558 (2019).
15. M. G. Behringer *et al.*, *Escherichia coli* cultures maintain stable subpopulation structure during long-term evolution. *Proc. Natl. Acad. Sci. U.S.A.* **115**, E4642-E4650 (2018).
16. M. G. Behringer *et al.*, Complex ecotype dynamics evolve in response to fluctuating resources. *mBio* **13**, e033467-21 (2022).
17. K. E. Kram *et al.*, Adaptation of *Escherichia coli* to long-term serial passage in complex medium: Evidence of parallel evolution. *mSystems* **2** (2017), 10.1128/mSystems.00192-16.
18. M. G. Behringer *et al.*, Trade-offs, trade-ups, and high mutational parallelism underlie microbial adaptation during extreme cycles of feast and famine. *Curr. Biol.* **34**, 1403-1413.e5 (2024).
19. C. Ratzke, J. Gore, Modifying and reacting to the environmental pH can drive bacterial interactions. *PLoS Biol.* **16**, e2004248 (2018).
20. M. J. Farrell, S. E. Finkel, The growth advantage in stationary-phase phenotype conferred by *rpoS* mutations is dependent on the pH and nutrient environment. *J. Bacteriol.* **185**, 7044-7052 (2003).
21. G. Sezonov, D. Joseleau-Petit, R. D'Arì, *Escherichia coli* physiology in Luria-Bertani broth. *J. Bacteriol.* **189**, 8746-8749 (2007).
22. R. Sánchez-Clemente, M. I. Guijo, J. Nogales, R. Blasco, Carbon source influence on extracellular pH changes along bacterial cell-growth. *Genes* **11**, 1292 (2020).
23. S. B. Worthan, R. D. P. McCarthy, M. G. Behringer, Case studies in the assessment of microbial fitness: Seemingly subtle changes can have major effects on phenotypic outcomes. *J. Mol. Evol.* **91**, 311-324 (2023).
24. T. A. Krulwich, G. Sachs, E. Padan, Molecular aspects of bacterial pH sensing and homeostasis. *Nat. Rev. Microbiol.* **9**, 330-343 (2011).
25. V. C. Santos, R. N. Araujo, L. A. D. Machado, M. H. Pereira, N. F. Gontijo, The physiology of the midgut of *Lutzomyia longipalpis* (Lutz and Neiva 1912): pH in different physiological conditions and mechanisms involved in its control. *J. Exp. Biol.* **211**, 2792-2798 (2008).
26. R. Lande, Evolution of phenotypic plasticity and environmental tolerance of a labile quantitative character in a fluctuating environment. *J. Evol. Biol.* **27**, 866-875 (2014).
27. P. A. O'Brien, K. M. Morrow, B. L. Willis, D. G. Bourne, Implications of Ocean acidification for marine microorganisms from the free-living to the host-associated. *Trend. Mar. Sci.* **3**, 47 (2016).
28. X. Yi, A. M. Dean, Phenotypic plasticity as an adaptation to a functional trade-off. *eLife* **5**, e19307 (2016).
29. M.-P. Castanié-Cornet *et al.*, Acid stress response in *Escherichia coli*: Mechanism of regulation of *gadA* transcription by RcsB and GadE. *Nucleic Acids Res.* **38**, 3546-3554 (2010).
30. P. A. Hoskisson, M. I. Hutchings, MtrAB-LpqB: A conserved three-component system in actinobacteria? *Trend. Microbiol.* **14**, 444-449 (2006).
31. I. Haneburger, A. Eichinger, A. Skerra, K. Jung, New insights into the signaling mechanism of the pH-responsive, membrane-integrated transcriptional activator CadC of *Escherichia coli*. *J. Biol. Chem.* **286**, 10681-10689 (2011).
32. A. Battesti, N. Majdalani, S. Gottesman, The RpoS-mediated general stress response in *Escherichia coli*. *Annu. Rev. Microbiol.* **65**, 189-213 (2011).
33. I. Hamdallah *et al.*, Experimental evolution of *Escherichia coli* K-12 at high pH and with RpoS induction. *Appl. Environ. Microbiol.* **84**, e00520-18 (2018).
34. J. Rebek, On the structure of histidine and its role in enzyme active sites. *Struct. Chem.* **1**, 129-131 (1990).
35. O. Röttschke, J. M. Lau, M. Hofstätter, K. Falk, J. L. Strominger, A pH-sensitive histidine residue as control element for ligand release from HLA-DR molecules. *Proc. Natl. Acad. Sci. U.S.A.* **99**, 16946-16950 (2002).
36. D. M. Williamson, J. Elferich, U. Shinde, Mechanism of fine-tuning pH sensors in proprotein convertases: Identification of a pH-sensing histidine pair in the propeptide of proprotein convertase 1/3. *J. Biol. Chem.* **290**, 23214-23225 (2015).
37. Y. Vercoulen *et al.*, A Histidine pH sensor regulates activation of the Ras-specific guanine nucleotide exchange factor RasGRP1. *eLife* **6**, e29002 (2017).
38. Y. Gerchman *et al.*, Histidine-226 is part of the pH sensor of NhaA, a Na⁺/H⁺ antiporter in *Escherichia coli*. *Proc. Natl. Acad. Sci. U.S.A.* **90**, 1212-1216 (1993).
39. B. A. Webb *et al.*, A histidine cluster in the cytoplasmic domain of the Na⁺/H⁺ exchanger NHE1 confers pH-sensitive phospholipid binding and regulates transporter activity. *JBC* **291**, 24096-24104 (2016).
40. Z. A. Szpiech *et al.*, Prominent features of the amino acid mutation landscape in cancer. *PLoS ONE* **12**, e0183273 (2017).
41. K. A. White *et al.*, Cancer-associated arginine-to-histidine mutations confer a gain in pH sensing to mutant proteins. *Sci. Signal.* **10**, eaam9931 (2017).
42. S. F. Elena, R. E. Lenski, Evolution experiments with microorganisms: The dynamics and genetic bases of adaptation. *Nat. Rev. Genet.* **4**, 457-469 (2003).
43. M. J. McDonald, Microbial experimental evolution—A proving ground for evolutionary theory and a tool for discovery. *EMBO Rep.* **20**, e46992 (2019).
44. G. Saxer *et al.*, Mutations in global regulators lead to metabolic selection during adaptation to complex environments. *PLoS Genet.* **10**, e1004872 (2014).
45. D. T. Fraebel, K. Gowda, M. Mani, S. Kuehn, Evolution of generalists by phenotypic plasticity. *iScience* **23**, 101678 (2020).
46. C. J. Cardinale *et al.*, Termination factor rho and its cofactors NusA and NusG silence foreign DNA in *E. coli*. *Science* **320**, 935-938 (2008).
47. J. M. Peters *et al.*, Rho and NusG suppress pervasive antisense transcription in *Escherichia coli*. *Genes Dev.* **26**, 2621-2633 (2012).
48. N. Sedlyarova *et al.*, sRNA-mediated control of transcription termination in *E. coli*. *Cell* **167**, 111-121.e13 (2016).
49. M. Delaune, E. Eveno, I. Simon, A. Schwartz, M. Boudvillain, A scalable framework for the discovery of functional helicase substrates and helicase-driven regulatory switches. *Proc. Natl. Acad. Sci. U.S.A.* **119**, e2209608119 (2022).
50. R. S. Washburn, M. E. Gottesman, Transcription termination maintains chromosome integrity. *Proc. Natl. Acad. Sci. U.S.A.* **108**, 792-797 (2011).
51. M. A. Kriner, A. Sevostyanova, E. A. Groisman, Learning from the leaders: Gene regulation by the transcription termination factor rho. *TIBS* **41**, 690-699 (2016).
52. L. Bossi, N. Figueroa-Bossi, P. Boulou, M. Boudvillain, Regulatory interplay between small RNAs and transcription termination factor Rho. *BBA-Gene Regul. Mech.* **1863**, 194546 (2020).
53. E. J. Steinmetz, T. Platt, Evidence supporting a tethered tracking model for helicase activity of *Escherichia coli* Rho factor. *Proc. Natl. Acad. Sci. U.S.A.* **91**, 1401-1405 (1994).
54. V. Molodtsov, C. Wang, E. Firlar, J. T. Kaelber, R. H. Ebricht, Structural basis of Rho-dependent transcription termination. *Nature* **614**, 367-374 (2023).
55. T. Kishimoto *et al.*, Transition from positive to neutral in mutation fixation along with continuing rising fitness in thermal adaptive evolution. *PLoS Genet.* **6**, e1001164 (2010).
56. O. Tenaillon *et al.*, The molecular diversity of adaptive convergence. *Science* **335**, 457-461 (2012).
57. A. Rodríguez-Verdugo, D. Carrillo-Cisneros, A. González-González, B. S. Gaut, A. F. Bennett, Different tradeoffs result from alternate genetic adaptations to a common environment. *Proc. Natl. Acad. Sci. U.S.A.* **111**, 12121-12126 (2014).
58. D. E. Deatherage, J. L. Kepner, A. F. Bennett, R. E. Lenski, J. E. Barrick, Specificity of genome evolution in experimental populations of *Escherichia coli* evolved at different temperatures. *Proc. Natl. Acad. Sci. U.S.A.* **114**, E1904-E1912 (2017).
59. S. M. Boyd *et al.*, Experimental evolution of copper resistance in *Escherichia coli* produces evolutionary trade-offs in the antibiotics chloramphenicol, bacitracin, and sulfonamide. *Antibiotics* **11**, 711 (2022).
60. P. L. Freddolino, H. Goodarzi, S. Tavazoie, Fitness landscape transformation through a single amino acid change in the rho terminator. *PLoS Genet.* **8**, e1002744 (2012).
61. R. J. F. Haft *et al.*, Correcting direct effects of ethanol on translation and transcription machinery confers ethanol tolerance in bacteria. *Proc. Natl. Acad. Sci. U.S.A.* **111**, E2576-E2585 (2014).
62. T. M. Conrad *et al.*, Whole-genome resequencing of *Escherichia coli* K-12 MG1655 undergoing short-term laboratory evolution in lactate minimal media reveals flexible selection of adaptive mutations. *Genome Biol.* **10**, R118 (2009).
63. M. D. Herron, M. Doebeli, Parallel evolutionary dynamics of adaptive diversification in *Escherichia coli*. *PLoS Biol.* **11**, e1001490 (2013).

64. M. G. Behringer *et al.*, Trade-offs, trade-ups, and high mutational parallelism underlie microbial adaptation to extreme feast/famine. *Curr. Biol.* **34**, 1403–1413.e5 (2024). 10.1101/2023.10.04.560893.
65. Y. Gao *et al.*, Systematic discovery of uncharacterized transcription factors in *Escherichia coli* K-12 MG1655. *Nucleic Acids Res.* **46**, 10682–10696 (2018).
66. A. J. Wolfe, The acetate switch. *Microbiol. Mol. Biol. Rev.* **69**, 12–50 (2005).
67. S. Cesar *et al.*, Bacterial evolution in high-osmolarity environments. *mBio* **11**, e01191–20 (2020).
68. P. Mitra, G. Ghosh, M. Hafeezunnisa, R. Sen, Rho protein: Roles and mechanisms. *Annu. Rev. Microbiol.* **71**, 687–709 (2017).
69. M. Damaghi, J. W. Wojtkowiak, R. J. Gillies, pH sensing and regulation in cancer. *Front. Physiol.* **4**, 370 (2013).
70. E. L. DiGiammarino *et al.*, A novel mechanism of tumorigenesis involving pH-dependent destabilization of a mutant p53 tetramer. *Nat. Struct. Mol. Biol.* **9**, 12–16 (2002).
71. C. Frantz *et al.*, Cofilin is a pH sensor for actin free barbed end formation: Role of phosphoinositide binding. *JCB* **183**, 865–879 (2008).
72. C.-H. Choi, B. A. Webb, M. S. Chimenti, M. P. Jacobson, D. L. Barber, pH sensing by FAK-His58 regulates focal adhesion remodeling. *JCB* **202**, 849–859 (2013).
73. V. Romiyó, J. W. Wilson, Phenotypes, transcriptome, and novel biofilm formation associated with the *ycdJ* gene. *Antonie van Leeuwenhoek* **113**, 1109–1122 (2020).
74. S. E. Maddocks, P. C. F. Oyston, Structure and function of the LysR-type transcriptional regulator (LTR) family proteins. *Microbiology* **154**, 3609–3623 (2008).
75. R. Shashni, M. Z. Qayyum, V. Vishalini, D. Dey, R. Sen, Redundancy of primary RNA-binding functions of the bacterial transcription terminator Rho. *Nucleic Acids Res.* **42**, 9677–9690 (2014).
76. K. Tsujimoto, M. Semadeni, M. Hullejt, L. Packer, Intracellular pH of halobacteria can be determined by the fluorescent dye 2',7'-bis(carboxyethyl)-5(6)-carboxyfluorescein. *BBRC* **155**, 123–129 (1988).
77. D. Molenaar, H. Bolhuis, T. Abee, B. Poolman, W. N. Konings, The efflux of a fluorescent probe is catalyzed by an ATP-driven extrusion system in *Lactococcus lactis*. *J. Bacteriol.* **174**, 3118–3124 (1992).
78. C. Riondet, R. Cachon, Y. Waché, G. Alcaraz, C. Diviès, Measurement of the intracellular pH in *Escherichia coli* with the internally conjugated fluorescent probe 5-(and 6-)carboxyfluorescein succinimidyl ester. *Biotechnol. Tech.* **11**, 735–738 (1997).
79. J. Heo, K. J. Thomas, G. H. Seong, R. M. Crooks, A microfluidic bioreactor based on hydrogel-entrapped *E. coli*: Cell viability, lysis, and intracellular enzyme reactions. *Anal. Chem.* **75**, 22–26 (2003).
80. E. R. Zinser, R. Kolter, Mutations enhancing amino acid catabolism confer a growth advantage in stationary phase. *J. Bacteriol.* **181**, 5800–5807 (1999).
81. S. Banerjee, J. Chalissery, I. Bandey, R. Sen, Rho-dependent transcription termination: More questions than answers. *J. Microbiol.* **44**, 11–22 (2006).
82. S. Festa, B. M. Coppotelli, I. S. Morelli, Bacterial diversity and functional interactions between bacterial strains from a phenanthrene-degrading consortium obtained from a chronically contaminated-soil. *Int. Biodeterior. Biodegrad.* **85**, 42–51 (2013).
83. P. Ileana *et al.*, "Soil quality problems associated with horticulture in the southern urban and peri-urban area of Buenos Aires, Argentina" in *Urban Horticulture—Necessity of the Future* (IntechOpen, 2020), 10.5772/intechopen.90351.
84. R. Ruvindy, R. A. White III, B. A. Neilan, B. P. Burns, Unravelling core microbial metabolisms in the hypersaline microbial mats of Shark Bay using high-throughput metagenomics. *ISME J.* **10**, 183–196 (2016).
85. R. A. White, H. L. Wong, R. Ruvindy, B. A. Neilan, B. P. Burns, Viral communities of Shark Bay modern stromatolites. *Front. Microbiol.* **9**, 1223 (2018).
86. A. Dostálová, P. Volf, Leishmania development in sand flies: Parasite–vector interactions overview. *Parasites Vectors* **5**, 276 (2012).
87. D. R. Speth *et al.*, Microbial communities of Auka hydrothermal sediments shed light on vent biogeography and the evolutionary history of thermophily. *ISME J.* **16**, 1750–1764 (2022).
88. K. Hama, T. Kunimaru, R. Metcalfe, A. J. Martin, The hydrogeochemistry of argillaceous rock formations at the Horonobe URL site, Japan. *Phys. Chem. Earth, Parts A/B/C* **32**, 170–180 (2007).
89. A. W. Hensdorf *et al.*, Potential for microbial H₂ and metal transformations associated with novel bacteria and archaea in deep terrestrial subsurface sediments. *ISME J.* **11**, 1915–1929 (2017).
90. J. M. Peters *et al.*, Rho directs widespread termination of intragenic and stable RNA transcription. *Proc. Natl. Acad. Sci. U.S.A.* **106**, 15406–15411 (2009).
91. E. T. Mohamed *et al.*, Generation of a platform strain for ionic liquid tolerance using adaptive laboratory evolution. *Microbiol. Cell Fact.* **16**, 204 (2017).
92. B. Du *et al.*, Adaptive laboratory evolution of *Escherichia coli* under acid stress. *Microbiology (Reading, MA)* **166**, 141–148 (2020).
93. Md. Hafeezunnisa, R. Sen, The rho-dependent transcription termination is involved in broad-spectrum antibiotic susceptibility in *Escherichia coli*. *Front. Microbiol.* **11**, 605305 (2020).
94. K. Bhardwaj *et al.*, Rho-dependent termination enables cellular pH homeostasis. *J. Bacteriol.* **206**, e0035623 (2024).
95. L. M. Stancik *et al.*, pH-dependent expression of periplasmic proteins and amino acid catabolism in *Escherichia coli*. *J. Bacteriol.* **184**, 4246–4258 (2002).
96. T. S. Gunasekera, L. N. Csonka, O. Pally, Genome-wide transcriptional responses of *Escherichia coli* K-12 to continuous osmotic and heat stresses. *J. Bacteriol.* **190**, 3712–3720 (2008).
97. S. M. Hug, B. S. Gaut, The phenotypic signature of adaptation to thermal stress in *Escherichia coli*. *BMC Evol. Biol.* **15**, 177 (2015).
98. C. H. Waddington, Genetic assimilation of an acquired character. *Evolution* **7**, 118–126 (1953).
99. M. Hafeezunnisa, P. I. R. Chhakhhuak, J. Krishnakumar, R. Sen, Rho-dependent transcription termination regulates the toxin–antitoxin modules of cryptic prophages to silence their expression in *Escherichia coli*. *FEBS Lett.* **595**, 2057–2067 (2021).
100. M. G. L. Eferink, K. J. Hellingwerf, W. N. Konings, The role of the proton motive force and electron flow in solute transport in *Escherichia coli*. *Eur. J. Biochem.* **153**, 161–165 (1985).
101. M. Sharma *et al.*, pH gradient reversal: An emerging hallmark of cancers. *Recent Pat. Anticancer Drug Discov.* **10**, 244–258 (2015).
102. T. Koltai *et al.*, "Chapter 5—How pH deregulation favors the hallmarks of cancer" in pH Deregulation as the Eleventh Hallmark of Cancer, T. Koltai *et al.*, Eds. (Academic Press, 2023), pp. 101–121, 10.1016/B978-0-443-15461-4.00008-4.
103. H. Lee, E. Popodi, H. Tang, P. L. Foster, Rate and molecular spectrum of spontaneous mutations in the bacterium *Escherichia coli* as determined by whole-genome sequencing. *Proc. Natl. Acad. Sci. U.S.A.* **109**, E2774–E2783 (2012).
104. J. A. Mosberg, C. J. Gregg, M. J. Lajoie, H. H. Wang, G. M. Church, Improving lambda red genome engineering in *Escherichia coli* via rational removal of endogenous nucleases. *PLoS ONE* **7**, e44638 (2012).
105. T. Baba *et al.*, Construction of *Escherichia coli* K-12 in-frame, single-gene knockout mutants: The Keio collection. *Mol. Syst. Biol.* **2**, 2006.0008 (2006).
106. A. Saragliadis, T. Trunk, J. C. Leo, Producing gene deletions in *Escherichia coli* by P1 transduction with excisable antibiotic resistance cassettes. *J. Vis. Exp.* **139**, 58267 (2018), 10.3791/58267.
107. B. R. Levin, F. M. Stewart, L. Chao, Resource-limited growth, competition, and predation: A model and experimental studies with bacteria and bacteriophage. *Am. Nat.* **111**, 3–24 (1977).
108. M. A. Schell, Molecular biology of the LysR family of transcriptional regulators. *Annu. Rev. Microbiol.* **47**, 597–626 (1993).
109. E.-A. Giannopoulou *et al.*, Crystal structure of the full-length LysR-type transcription regulator CbnR in complex with promoter DNA. *FEBS J.* **288**, 4560–4575 (2021).
110. M. Boudvillain, C. Walmacq, A. Schwartz, F. Jacquinet, "Simple enzymatic assays for the in vitro motor activity of transcription termination factor Rho from *Escherichia coli*" in *Helicases: Methods and Protocols*, M. Abdelhaleem, Eds. (Humana Press, Totowa, NJ, 2010), pp. 137–154, 10.1007/978-1-60327-355-8_10.
111. E. Soares, A. Schwartz, M. Nollmann, E. Margeat, M. Boudvillain, The RNA-mediated, asymmetric ring regulatory mechanism of the transcription termination Rho helicase decrypted by time-resolved nucleotide analog interference probing (trNAIP). *Nucleic Acids Res.* **42**, 9270–9284 (2014).
112. C. Nadiras, E. Eveno, A. Schwartz, N. Figueroa-Bossi, M. Boudvillain, A multivariate prediction model for Rho-dependent termination of transcription. *Nucleic Acids Res.* **46**, 8245–8260 (2018).
113. F. D'Hegyère, A. Schwartz, F. Coste, B. Castaing, M. Boudvillain, ATP-dependent motor activity of the transcription termination factor Rho from *Mycobacterium tuberculosis*. *Nucleic Acids Res.* **43**, 6099–6111 (2015).
114. H. Z. Low *et al.*, Fast and easy phage-tagging and live/dead analysis for the rapid monitoring of bacteriophage infection. *Front. Microbiol.* **11**, 602444 (2020).
115. B. Roeder, M. Wagner, P. Rossmanith, Autonomous growth of isolated single *Listeria monocytogenes* and *Salmonella enterica* serovar typhimurium cells in the absence of growth factors and intercellular contact. *Appl. Environ. Microbiol.* **76**, 2600–2606 (2010).
116. R. E. Lenski *et al.*, Adaptation and divergence during 2,000 generations. *Am. Nat.* **138**, 1315–1341 (1991).
117. Z. Zhang *et al.*, Protein sequence similarity searches using patterns as seeds. *Nucleic Acids Res.* **26**, 3986–3990 (1998).
118. J. S. Papadopoulos, R. Agarwala, COBALT: Constraint-based alignment tool for multiple protein sequences. *Bioinformatics* **23**, 1073–1079 (2007).

Supporting Information for

Evolution of pH-sensitive transcription termination in *Escherichia coli* during adaptation to repeated long-term starvation.

Sarah B. Worthan, Robert D. P. McCarthy, Mildred Delaleau, Ryan Stikeleather, Benjamin P. Bratton, Marc Boudvillain, and Megan G. Behringer

Corresponding Author: Megan G. Behringer
E-mail: megan.g.behringer@vanderbilt.edu

This PDF file includes:

Supplemental Methods
Figures S1 to S12
Table S1

Supplemental Methods

Long-Term Survival Assays and Culture pH

We assessed long-term survival of the WT, *rho* R109H, $\Delta ydcI$, and *rho* R109H/ $\Delta ydcI$ strains through periodic quantification of population cellular density via viable plate counts. We inoculated 3 replicate overnight cultures of WT, *rho* R109H, $\Delta ydcI$, and *rho* R109H/ $\Delta ydcI$ strains in 10 mL of LB broth each originating from a separate colony from an LB agar plate freshly prepared from frozen glycerol stocks and incubated them for 18 hours at 37°C. The long-term survival assay was initiated by aliquoting 100 μ L of each overnight culture into 16 individual culture tubes filled with 10 mL of fresh LB broth with each tube representing a sampling time point. We incubated the cultures at 37°C, shaken upright at 180 rpm until the appropriate sampling time point. We set up individual cultures for each sampling time point, as vortexing and resampling of the same culture tube has been shown to alter fitness outcomes. We left cultures undisturbed during incubation except for a brief period every 10 days when the culture tubes were gently removed from the incubator and sterile diH₂O was added to achieve a volume of 10 mL in efforts to counteract evaporation. We performed viable cell plate counts at time 0 by sampling the tubes immediately following inoculation. Thereafter, the population density was sampled after 1, 4, and 7 days, followed by every 7 days until 100 days. At the appropriate sampling time point, the corresponding culture tubes were removed from the incubator and gently vortexed. We then removed 100 μ L from the cultures and performed serial dilutions in PBS. We plated a 100 μ L aliquots of the dilutions on LB agar plates and enumerated the colonies from countable plates after 24 hours of incubation at 37°C. We also removed 1 mL aliquots from the culture tubes during sampling and removed the cells via centrifugation at 2500 x g for 5 minutes. We then measured the pH of the resulting supernatant using the Thermo Scientific Orion Star A214 pH meter.

Growth Analyses

We assessed growth of the *rho* R109H strain in conditions that previously produced other experimentally evolved *rho* mutations, including temperature stress, exposure to ethanol, and osmotic stress. All growth analyses were performed in 96-well plates, and we used a Synergy H1 Plate Reader (Biotek) to analyze growth. A volume of 150 μ L of LB broth was inoculated with 1.5 μ L of overnight culture in each well so that every strain had three biological replicates. The 96-well plate underwent an 18-hour program at 37 °C with continuous orbital shaking at 807 c.p.m. Initial and final absorbance (600 nm) readings were taken, as well as intermittent absorbance readings every 15 min. Temperature stress was evaluated by growing the strains at three different temperatures: 32 °C, 37 °C, and 42 °C. Exposure to ethanol was measured by supplementing ethanol into LB broth using three different concentrations: 4%, 6%, and 7%. Finally, osmotic stress was evaluated in two ways: by supplementing cultures with NaCl (0.1 M NaCl, 0.2 M NaCl, 0.5 M NaCl, and 1.0 M NaCl) and by supplementing cultures with sucrose (0.1 M sucrose, 0.2 M sucrose, 0.5 M sucrose, and 1.0 M sucrose). Growth curve parameters and statistics were calculated with the R package Growthcurver (v.0.3.1) which fits growth data to a logistic model.

Supplemental Figures

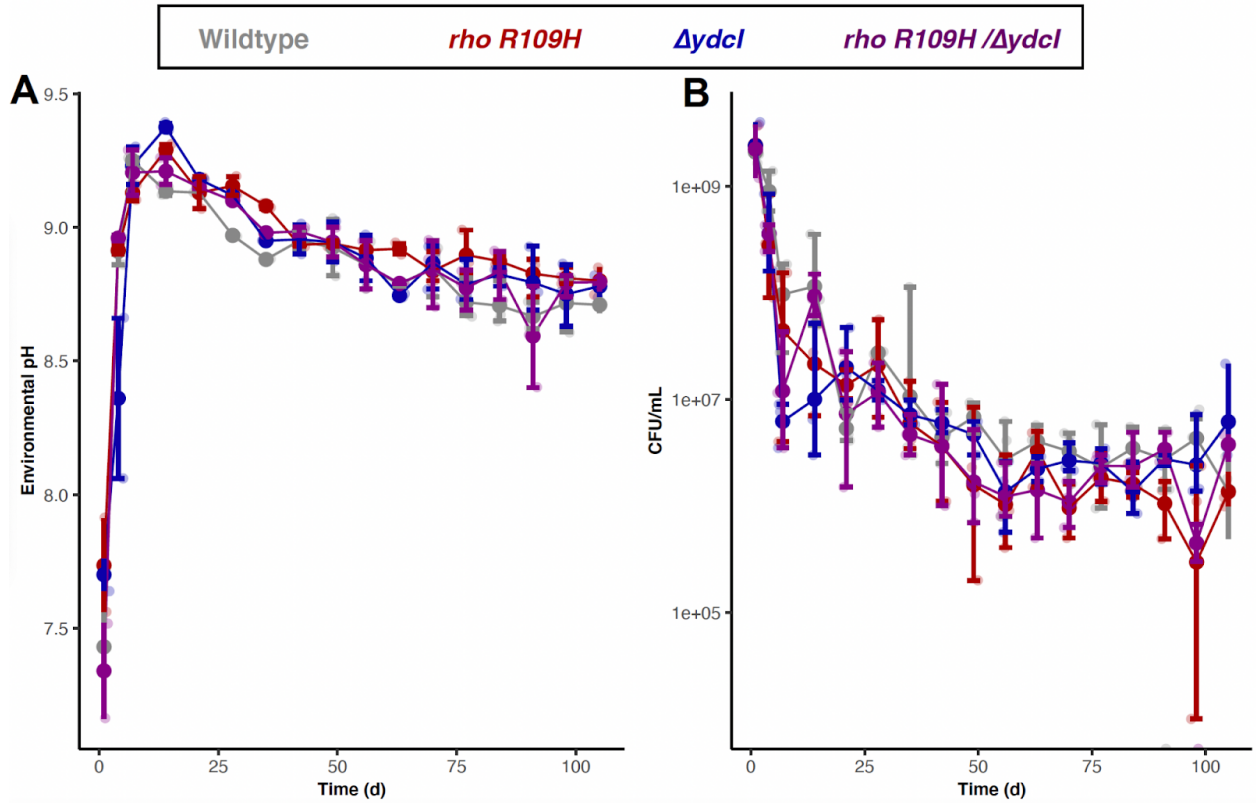


Fig S1: Culture pH and Survival over 100 days. (A). The medium pH (environmental pH) of cultures containing WT, *rho R109H*, $\Delta ydcI$, and *rho R109H/\Delta ydcI* were determined over the course of 100 days. **(B).** Survival of cultures, as measured by viable plate counts (CFU/mL), containing WT, *rho R109H*, $\Delta ydcI$, and *rho R109H/\Delta ydcI* were determined over the course of 100 days. Each data point represents the median of 3 biological replicate cultures. Error bars denote 95% confidence intervals.

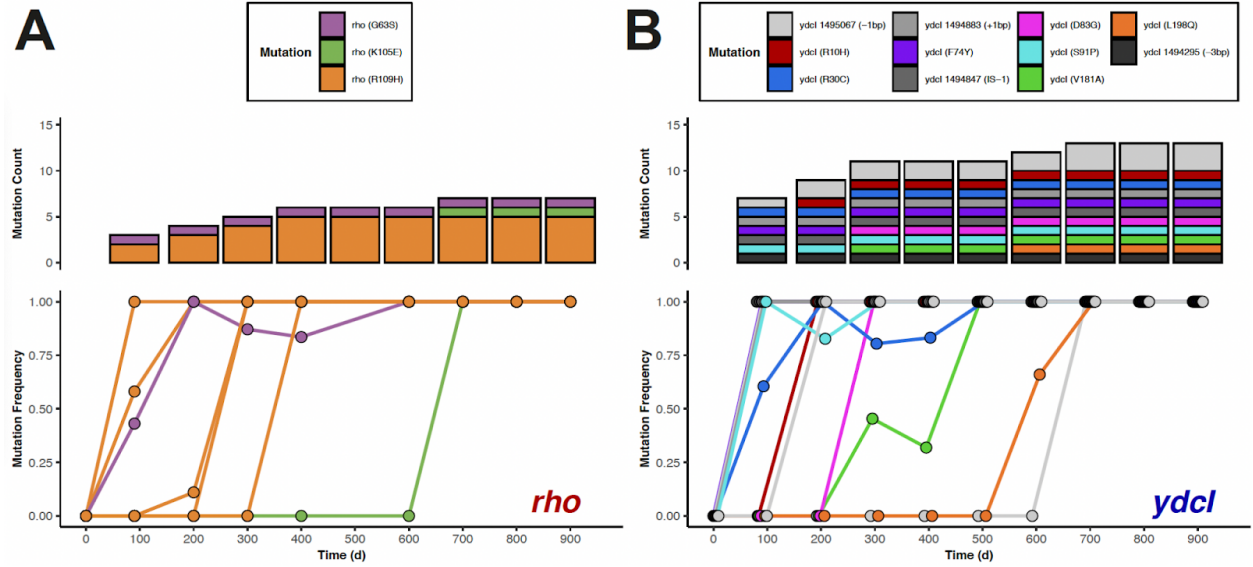


Fig S2: Mutation dynamics in *rho* and *ydcI* over 900 days of experimental evolution. The number (mutation count) and frequency of mutations in (A). *rho* and (B). *ydcI* genes in experimentally evolved populations over 900 days of RLTS. Colors in plots correspond to different alleles defined in the legends.

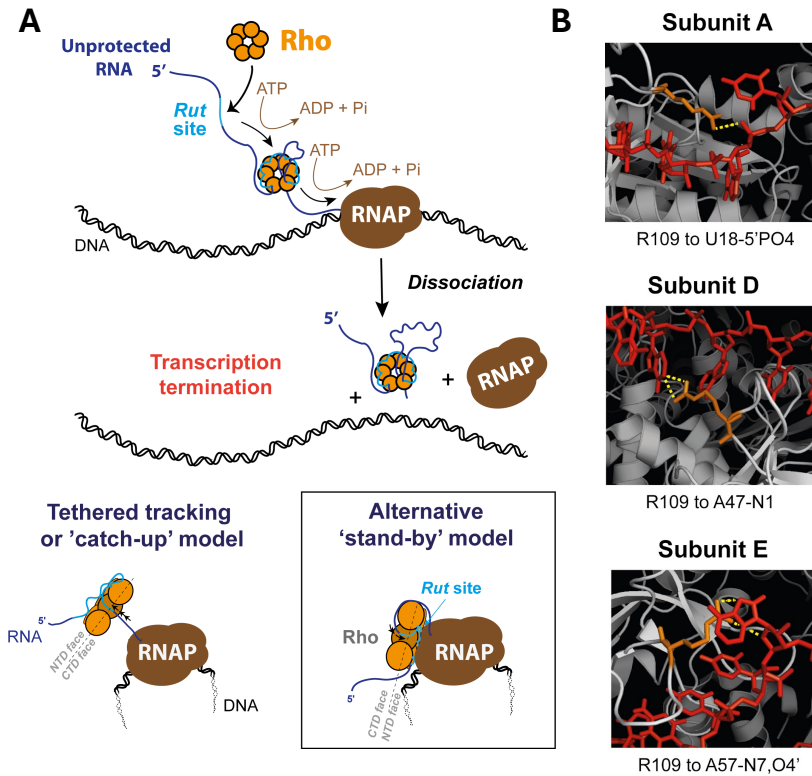


Fig S3: Molecular mechanism of Rho-dependent Termination. (A) Schematic depiction of Rho-dependent termination. The Rho hexamer binds an accessible *Rut* site in the nascent RNA transcript using its Primary Binding Site (PBS). This initial interaction drives the RNA chain into the hexamer central channel where the RNA binds Rho's Secondary binding Site (SBS). This triggers the closure and catalytic activation of the Rho ring, which can then translocate along the RNA, towards the RNA polymerase, in an ATP-dependent manner. Once Rho catches the RNA polymerase, it triggers dissociation of the transcription elongation complex. This 'tethered tracking' or 'catch-up' model is supported by a recent cryoEM reconstruction of the *E. coli* pre-termination complex (Molodtsov 2023 PMID: 36697824). However, other cryoEM reconstructions support an alternative 'stand-by' model (box) wherein Rho is pre-bound to the RNA polymerase in an inverted 'CTD face to NTD face' orientation (Said 2021 PMID: 33243850; Hao, 2022 PMID: 33296676). In this model, Rho continuously scans the RNA chain and initiates termination only when it recognizes a *Rut* site. Recent single-molecule fluorescence (Song 2022 PMID: 35351884) and cryoEM (Murayama, 2023 PMID: 36753546) studies propose that both models in fact coexist and contribute to Rho-dependent termination, the catch-up pathway being the fastest while the stand-by pathway is favored by long transcriptional pauses *in vitro* (Song 2023 PMID: 36762473). (B). Rho primary RNA binding site highlighting position of residue R109. Direct R109 (orange) to RNA (red) contacts, indicated in yellow, in Rho subunits observed in PDB# 8E6W clearly illustrates R109 as part of the RNA primary binding site.

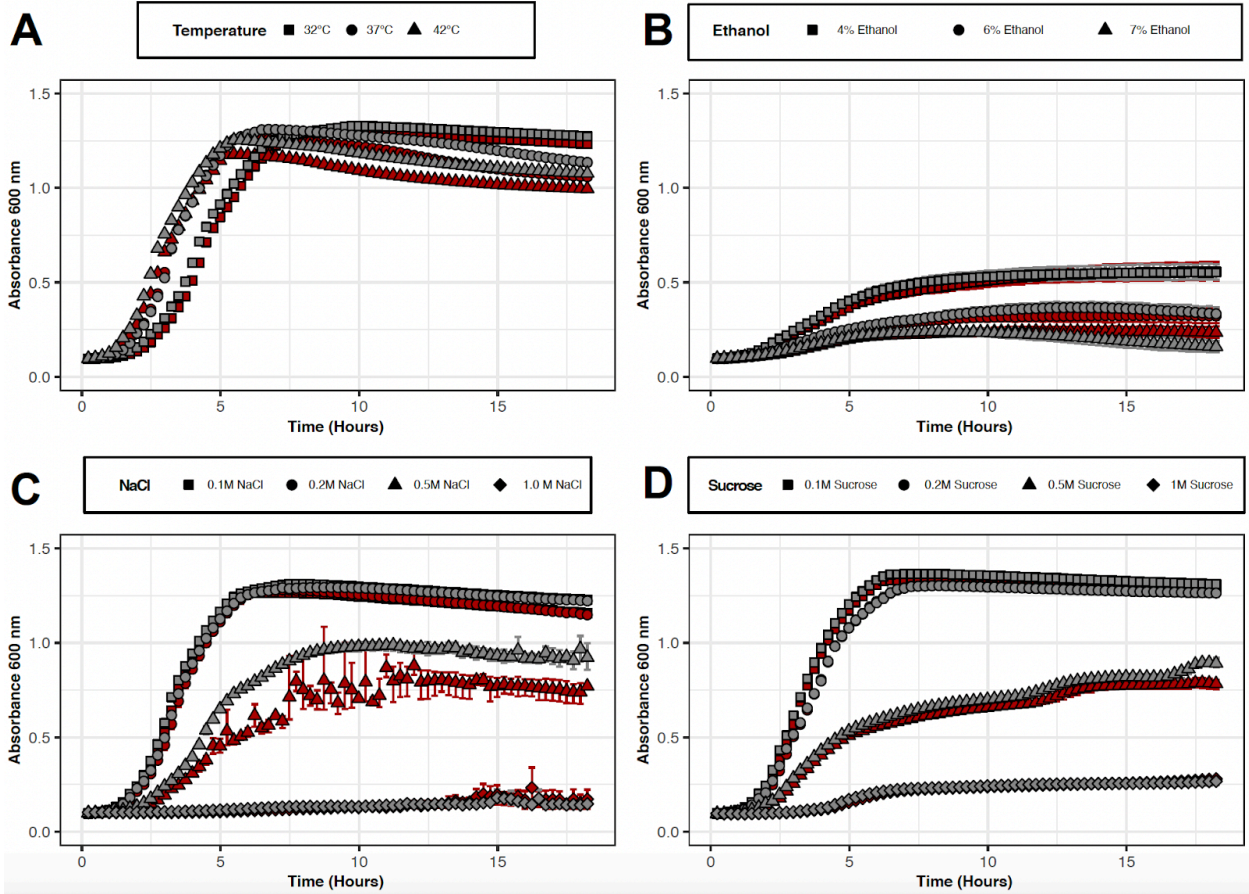


Fig S4: Growth Analyses of *rho* R109H in conditions that previously produced other experimentally evolved *rho* mutations. WT (gray) and *rho* R109H (red) cultures were grown for 18 hours in LB broth at varying (A). temperatures or supplemented with several concentrations of (B). ethanol, (C). NaCl, and (D). sucrose. Each data point represents the median of three biological replicates. Error bars represent 95% confidence intervals.

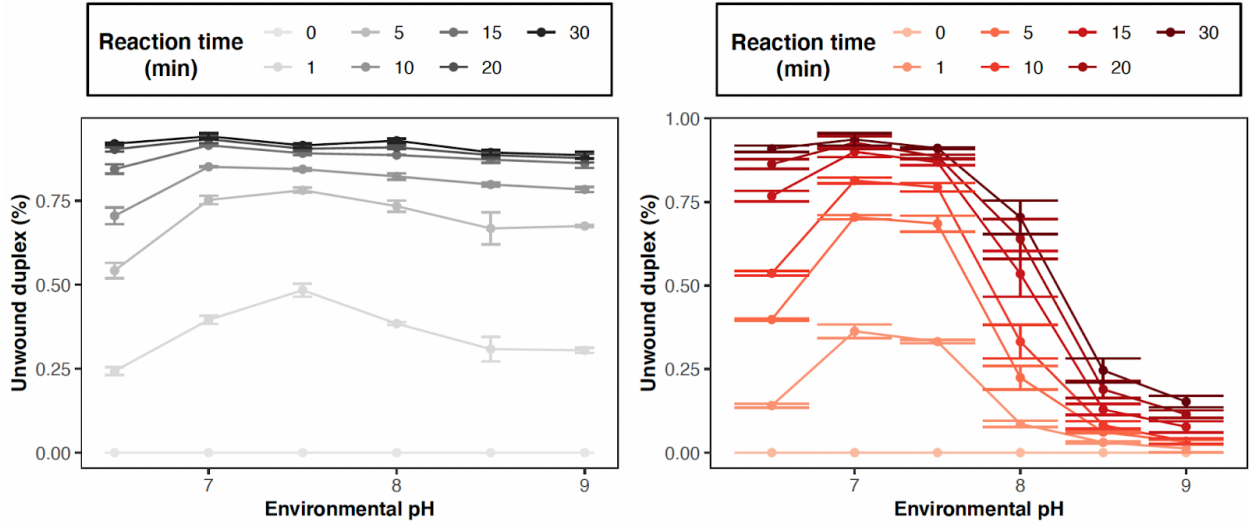


Fig S5: Helicase activity of Rho to unwind a RNA:DNA duplex. Percent of unwound duplex over the reaction time (min) across increasing environmental pH conditions for Rho⁺ (gray scale) and Rho^{R109H} (red scale) proteins. Each data point represents the median of 2 biological replicates with error bars representing 95% confidence intervals.

Transcription termination

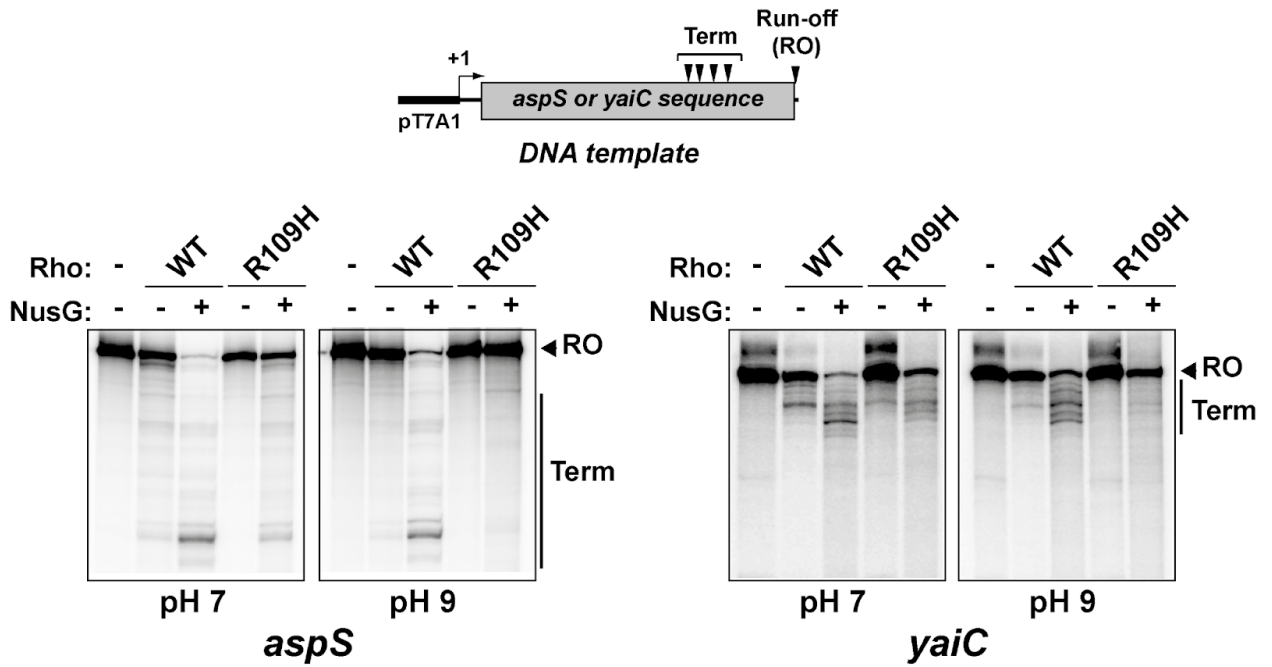


Fig S6: Termination with the R109H mutant is also dependent on pH at NusG-stimulated terminators. Transcription termination *in vitro* activity of Rho⁺ (WT) and Rho^{R109H} (R109H) proteins at NusG-stimulated terminators in *aspS* and *yaiC* genes in pH 7 and pH 9 conditions. Schematic above gel images denotes the design of DNA template used for the termination activity assay.

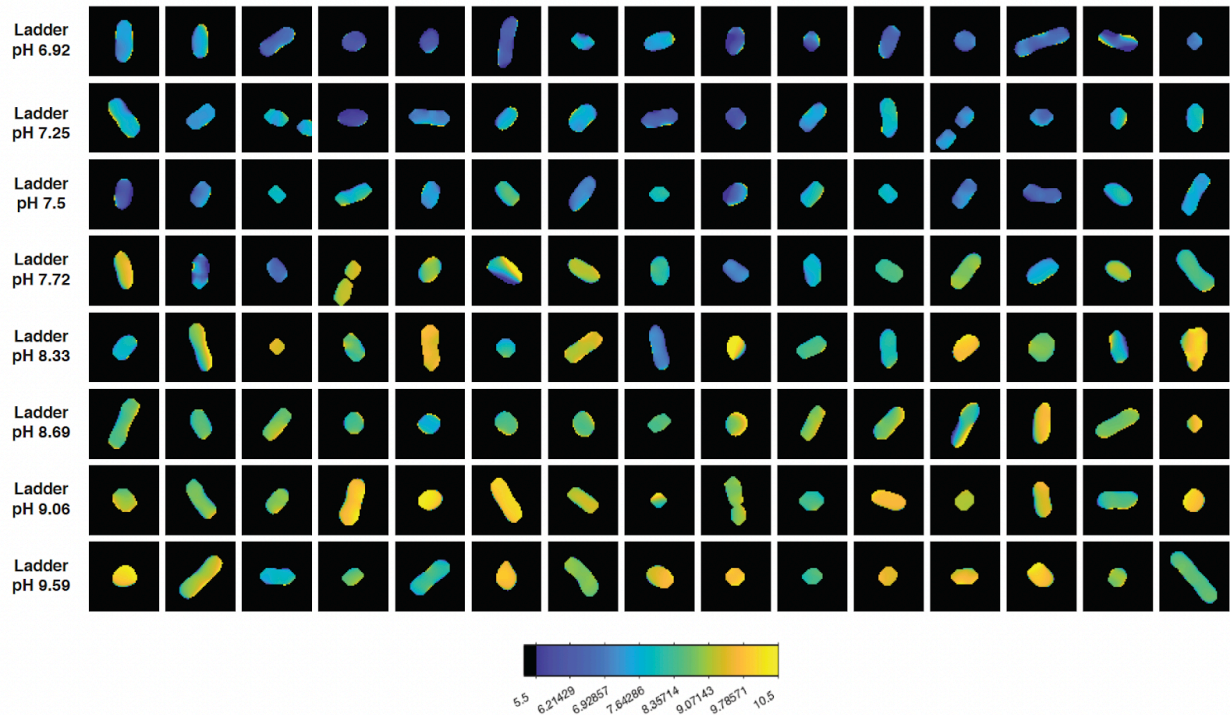


Fig S7: Control Ladder for measurement of intracellular pH. Microscopic images of all replicate WT cells treated with nigericin, yielding the intracellular and environmental pH equal, used to produce calibration curve. Color of cells correspond to the cellular pH as denoted on the scale below microscopic images. Each image is cropped to 5.5 x 5.5 μm .

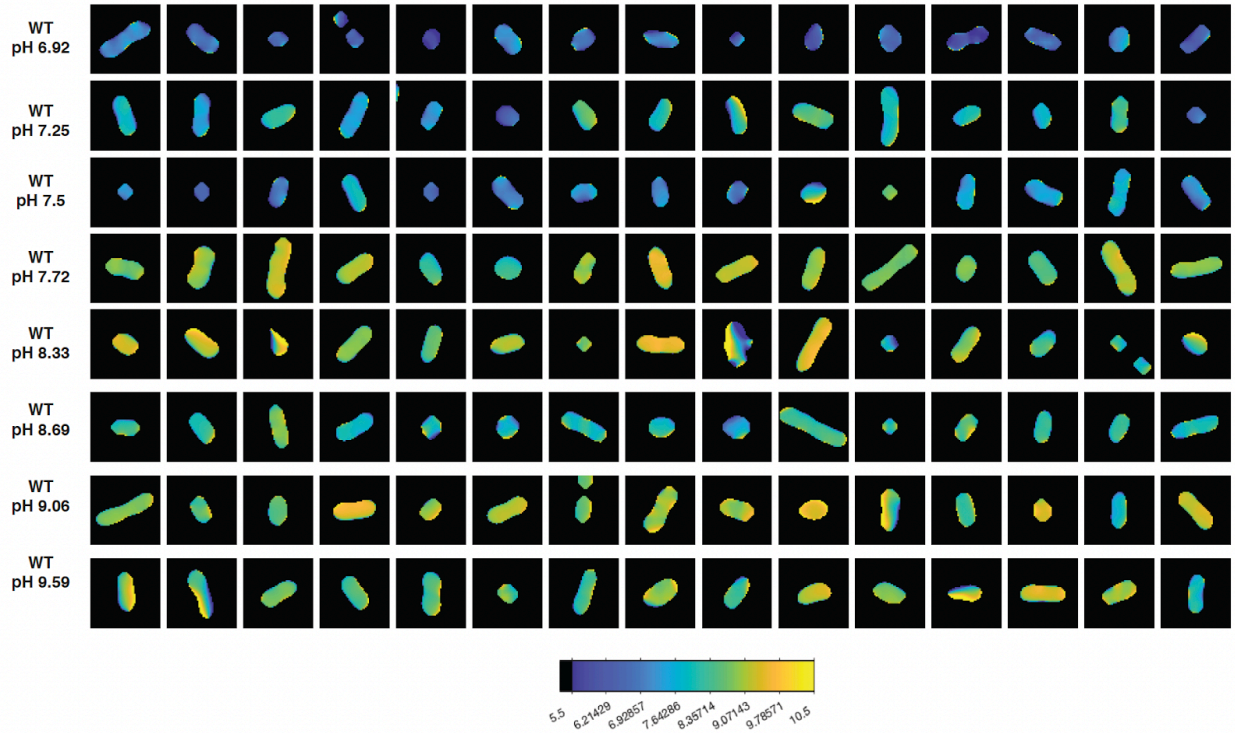


Fig S8: Intracellular pH of WT cells across an environmental pH gradient. Microscopic images of all replicate WT cells stained with BCECF in a range of pH adjusted buffers. Color of cells correspond to the cellular pH as denoted on the scale below microscopic images. Each image is cropped to 5.5 x 5.5 μm .

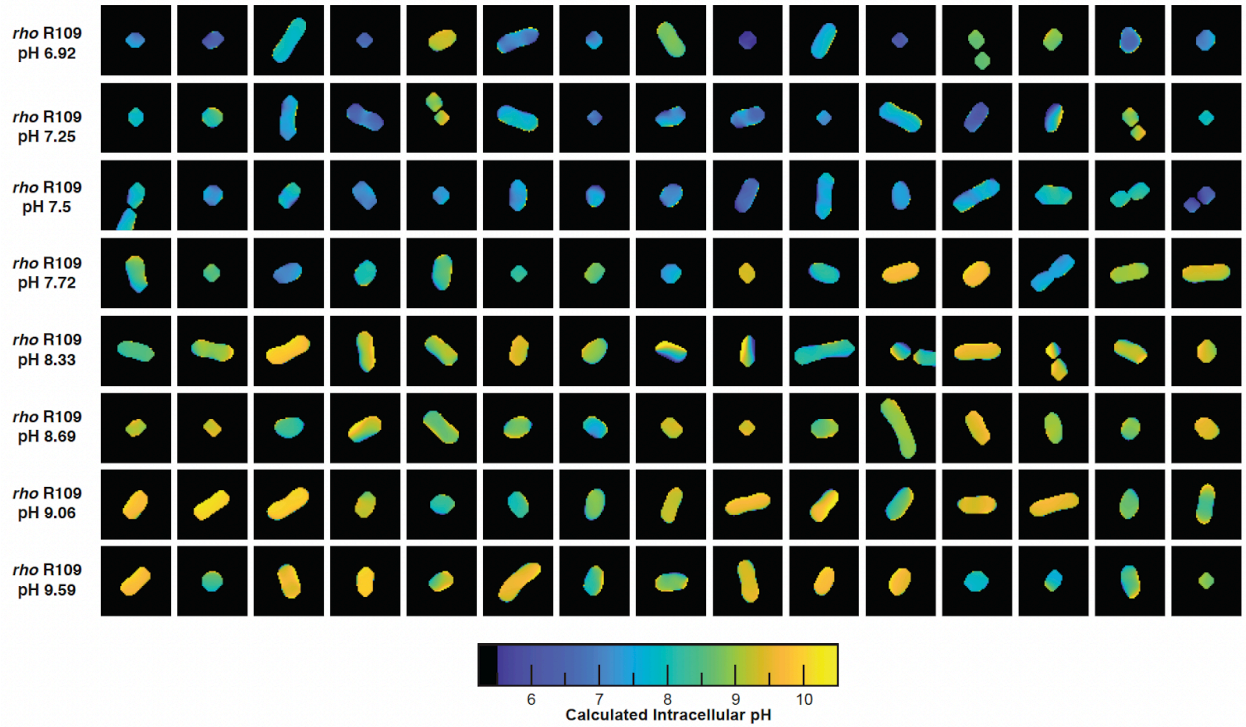


Fig S9: Intracellular pH of *rho* R109H cells across an environmental pH gradient. Microscopic images of all replicate *rho* R109H cells stained with BCECF in a range of pH adjusted buffers. Color of cells correspond to the cellular pH as denoted on the scale below microscopic images. Each image is cropped to 5.5 x 5.5 μm .

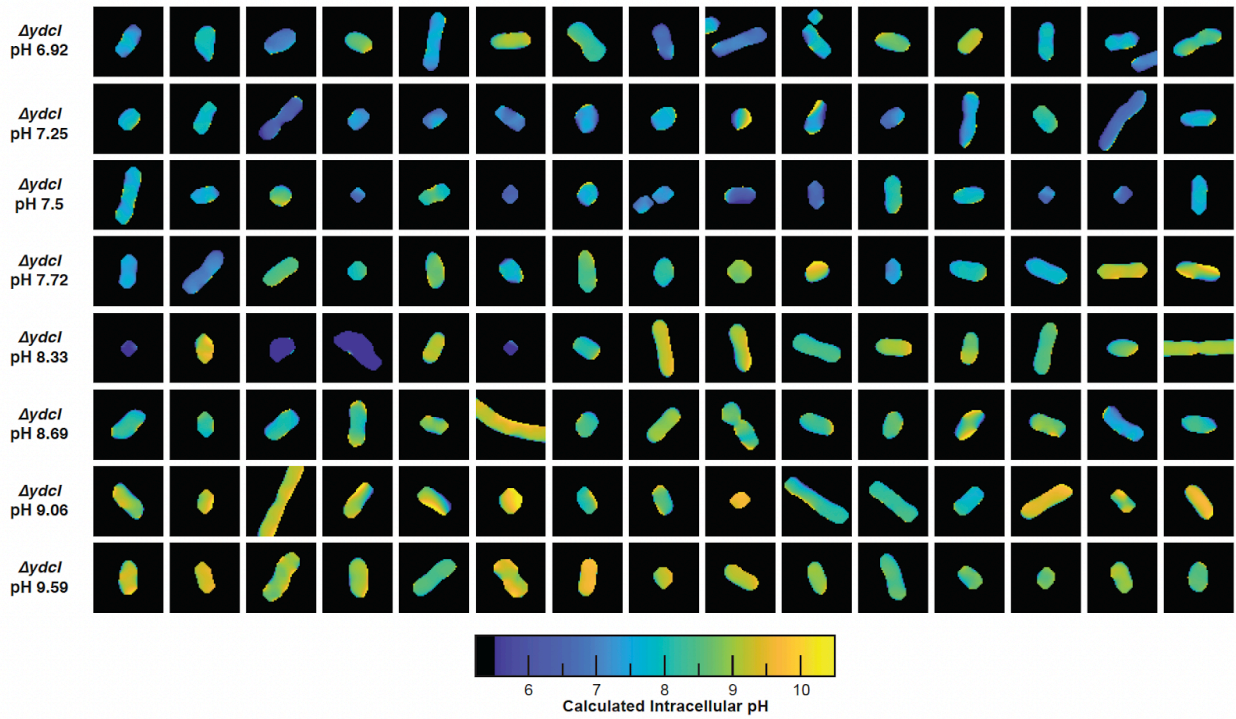


Fig S10: Intracellular pH of $\Delta ydcI$ cells across an environmental pH gradient. Microscopic images of all replicate $\Delta ydcI$ cells stained with BCECF in a range of pH adjusted buffers. Color of cells correspond to the cellular pH as denoted on the scale below microscopic images. Each image is cropped to $5.5 \times 5.5 \mu\text{m}$.

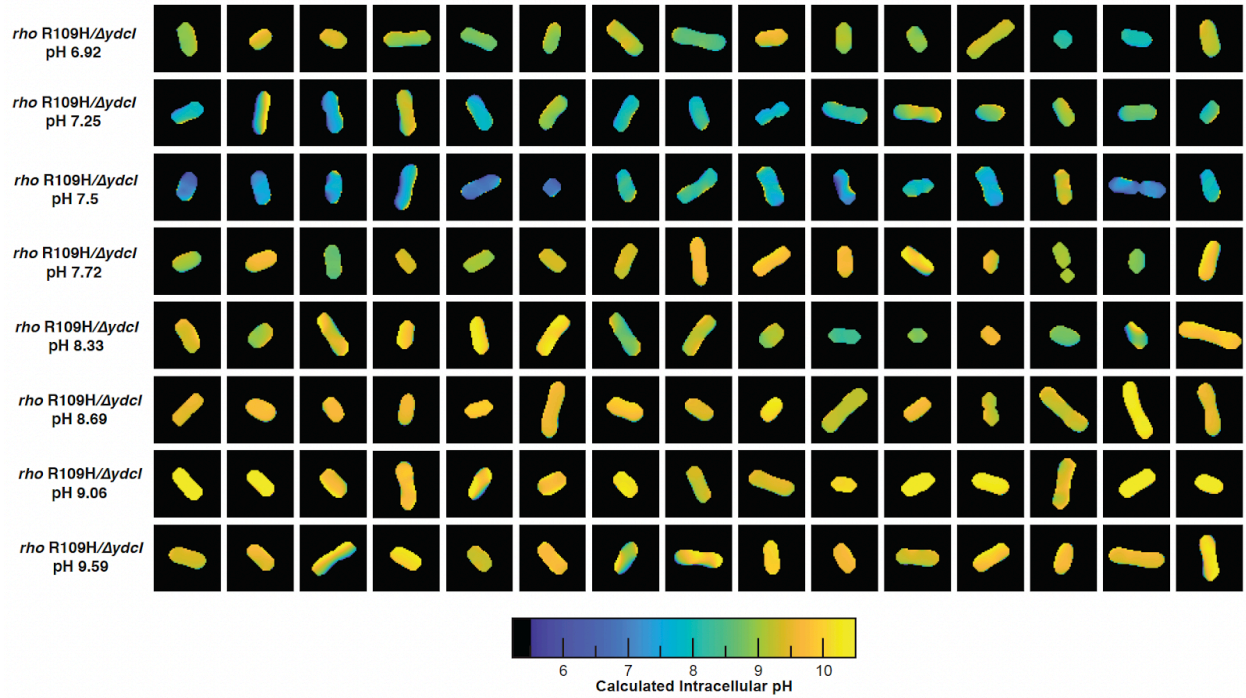


Fig S11: Intracellular pH of *rho* R109H/ Δ *dydc1* cells across an environmental pH gradient. Microscopic images of all replicate *rho* R109H/ Δ *dydc1* cells stained with BCECF in a range of pH adjusted buffers. Color of cells correspond to the cellular pH as denoted on the scale below microscopic images. Each image is cropped to 5.5 x 5.5 μ m.

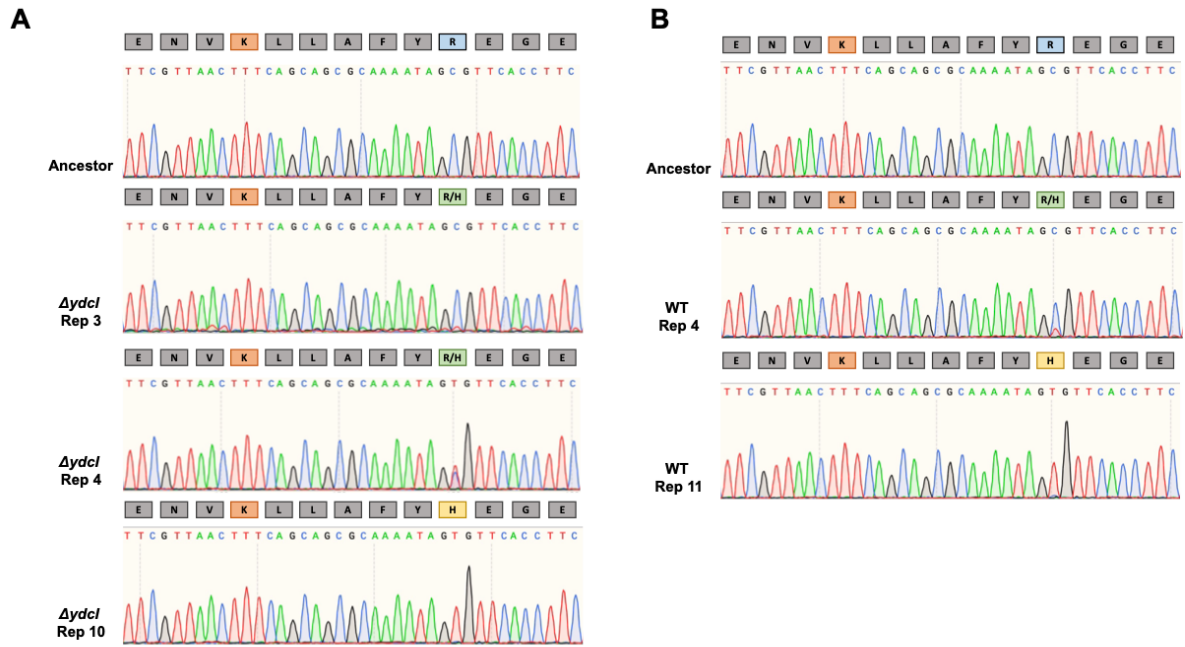


Fig S12: Replaying one cycle of RLTS regime results in emergence of *rho* R109H mutation in initial $\Delta ydcI$ and WT genetic background. Portion of Sanger sequences containing the nucleotide sequence corresponding to the primary RNA binding site in Rho (Amino acid residues 106-118) with single letters above traces corresponding to the amino acid sequence. K105 residue is marked in orange, while R109 residue is marked in blue. The green R/H denotes a polymorphism at that position as indicated by the Sanger sequence. Yellow H denotes fixation of the R109H allele.

Table S1. Relevant genotypes and phenotypes of populations adapted to 100-day feast/famine cycles

Population	<i>rho</i>	<i>ydcl</i>	AraBAD	MMR
501	R109H	-3bp	AraBAD ⁺	MMR ⁺
503	K105E	-1bp	AraBAD ⁻	MMR ⁺
504	R109H	R10H	AraBAD ⁺	MMR ⁻
506	WT	V181A	AraBAD ⁻	MMR ⁻
508	WT	IS1	AraBAD ⁻	MMR ⁺
509	WT	WT	AraBAD ⁺	MMR ⁻
511	R109H	D83G	AraBAD ⁻	MMR ⁻
512	WT	WT	AraBAD ⁺	MMR ⁺
513	WT	F74Y	AraBAD ⁺	MMR ⁺
515	WT	-1bp	AraBAD ⁻	MMR ⁺
516	G63S	R30C	AraBAD ⁺	MMR ⁻
518	R109H	+1bp	AraBAD ⁻	MMR ⁻
520	WT	L198Q	AraBAD ⁻	MMR ⁺
521	WT	WT	AraBAD ⁺	MMR ⁻
523	R109H	S91P	AraBAD ⁻	MMR ⁻
524	WT	-1bp	AraBAD ⁺	MMR ⁺